공학박사 학위논문

Preparation and Characterization of Nanostructured Electrode Materials via Polymer-Mediated Synthesis

고분자 매개체를 이용한 나노구조체 전극물질 제조 및 특성연구

2014년 8월

서울대학교 대학원

화학생물공학부

김 길 표

Abstract

Preparation and Characterization of Nanostructured Electrode Materials via Polymer-Mediated Electrodeposition

Gil-Pyo Kim

Chemical Convergence for Energy & Environment

School of Chemical and Biological Engineering

The Graduate School

Seoul National University

Popularization of electric vehicles and portable electornic device stimulates the development of energy storage and conversion devices, such as Li-ion batteries (LIBs), supercapacitors, and fuel cells (FCs), toward high power and energy density and high safty, which significantly depends upon the advancement of new materials used in these systems. Moreover, electrode materials play an essential role in effiency, clean and versatile use of energy. Therefore, a wide range of nanostructured electrode materials have received great attention from research to meet the demands of high performance and clean energy source. Among the several general strategies for making nanostructured electrode materials, notable progress in the study of organic/inorganic hybrid materials has been made in recent years. Although various approaches have been employed to prepare the nanostructured hybrid materials, most of the currently proposed methods obviously involve highly toxic chemicals or high temperatures and, moreover, high energy consumption

and multi-step processes are required. Consequently, a more efficient process for production is needed.

In this dissertation, the nanostructured carbon/metal oxide hybrid materials prepared by polymer-mediated strategies are proposed as electrode materials for energy storage. This facile and scalable synthesis is using polyethyleneimine (PEI) as a stabilizer, template, and active site for anchoring metal precursors and agarose gel as a carbon source and mediation for the preferential growth of metal oxides. Details are as follows:

Firstly, graphene/Co_3O_4 and NiO thin films were prepared by the directly co-electrodeposition using PEI-assisted strategy. Water-soluble cationic PEI chains grafted onto graphene oxides (GOs) acted as a kind of trapping agent for cationic metal ions, which plays a key role in sequential complexation between GOs and cationic precursor ions such as Co^{2+} and Ni^{2+}. For the formation of PEI modified GOs (PEI-GOs) and metal ion complexes, the PEI-GOs dispersion was mixed with aqueous phase of $Co(NO_3)_2$ and $Ni(NO_3)_2$, respectively. And then, the solution was used as the plating bath for coelectrodeposition. Results showed that the graphene and metal oxides were uniformly distributed on the surface of the substrate. The prepared graphene/metal oxide films were employed as an anode material for LIBs, and it exhibited not only an enhanced cycleability but also high electronic conductivity.

Secondly, a simple strategy for the synthesis of Co_3O_4 and NiO/carbonaceous matrix composite using an agarose gel-mediated electrodeposition is described to achieve large reversible capacity and long cycle stability of electrode. The close-packed and porous sturctures were formed by a preferential growth mechanism within a short time. Results of X-ray diffraction (XRD) and fourier transform infrared spectroscopy (FT-IR) proved the preferential (111) growth of metal oxide embedded in carbonaceous matrix. As an anode material for lithium ion batteries, this novel

structure played a positive role in producing a material with a large reversible capacity, high conductivity, and long cyclic stability. The high reversible capacity was maintained at an elevated current density. The results indicated the existence of a synergetic effect between the porous metal oxide layers and the conductive matrix in the composite.

The results suggest that the concept proposed herein can be effectively used to overcome a bottleneck problem associated with the production of organic/inorganic hybrid materials with nanostructure.

Keywords: Polyethyleneimine, Agarose, Cobalt oxide, Nickel Oxide, Nanostructured electrode, Lithium-ion battery

Student Number: 2011-30797

Contents

List of Figures

Chapter 1. Introduction

1.1 Lithium-ion battery for energy storage system

Energy is one of the most important topics in this century than it was in the last. With the increasingly worsened environmental pollution and the rapid depletion of fossil fuels caused by vast fossil-fuel consumption, power generation using renewable and clean energy sources has been considered as a solution for the sustainable development of our economy and society. In addition, the use of energy storage system has rapidly increased and its consumption manner is diversified due to the development of modern industries and the increase of global population, which leads to the system to become even more complex [1-6]. In a typical system, one type of energy is converted into another form of energy that can be stored and converted for desirable use. Therefore, various energy storage and conversion system are being needed for proper utilization of different energy sources.

Lithium-ion battery (LIB), with the advantages of light, compact, and high-performance, are being developed as electrical power sources from hybrid electric vehicles to portable applications [1,2]. As shown in Figure 1-1, a LIB contains a graphite negative electrode, a positive electrode formed by lithium metal oxide ($LiMO_2$), and a non-aqueous liquid electrolyte. The charge and discharge processes involve a reversible insertion/extraction of lithium ions between the two electrodes. The lithium intercalation/deintercalation process occurring with a flow of ions through the electrolyte is accompanied by a

redox reaction assisted by a flow of electrons through the external circuit [1]. The capacity of LIBs is given by their ability to uptake Li-ions wihout suffering irreversible structural changes. Therefore, the pristine structure needs to be maintained during the reaction in order to maintain good reversibility of the Li ions [3].

As there is growing interest in energy storage systems with both high power and a high energy density for possible applications in power tools or electric vehicles, the principal challenges facing the development of LIB are cost, safety, rate capability, and service life. In this regards, many researches have been focused on the development of the nanostructured thin film electrode materials.

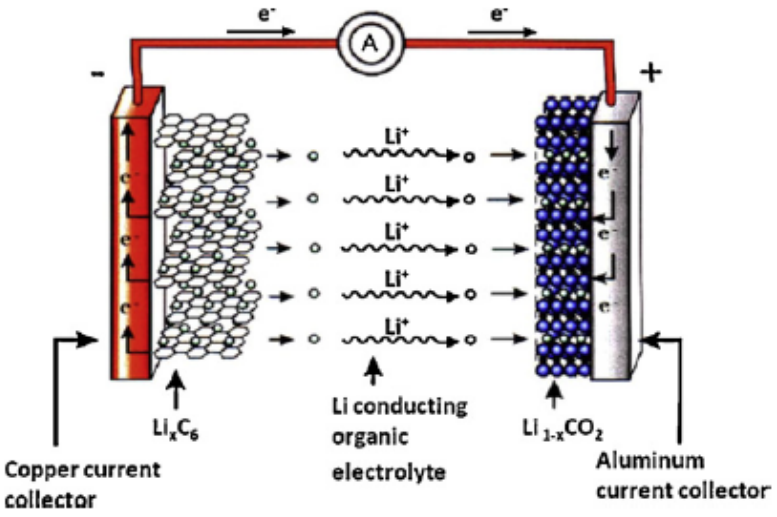

Figure 1-1. Schematic representation of a lithium-ion battery. Negative electrode (graphite), positive electrode ($LiCoO_2$), separated by a non-aqueous liquid electrolyte [5].

1.2 Nanostructured electrode material

Fully flexible electronics have been rapidly developed. To achieve the flexible system, flexible electrodes are indispensable. As reduced weight, volume, and long use performance of batteries are directly connected to the energy density, research on the flexible LIB should focus not only on providing flexible components but also on achieving a higher energy density. Design and development of new electrode materials that can lower the cost, increase the efficiency, and improve the stability can be of both the scientific and the practical significance. In this sence, nanostructured materials provide great promise due to the unique properties endowed by confining their dimensions and the combination of bulk and surface properties to the overall behavior [1]. The 1-, 2-, and 3D nanostructured electrode materials can be materialized by the several strategies such as nano-/micro combination, hybridization, pore-structure control, configuration design, surface modification, and composition optimization [3,4]. These electrode materials with nanoarchitectures exhibit much better electrochemical properties than those dense counterparts due to the large surface area and the highly efficient transport of electrolytic ions and intermediate reactants. However, while desirable properties are achieved for the subtly designed energy storage materials, drawbacks still exist. In addition, the powder typed active materials need to be mixed with carbon and polymer binders. This process risks negating the benefits associated with the reduced particle size and introduces supplementary, undesirable interfaces. For these reasons, the direct growth of

nanostructured materials on various substrates, especially on flexible substrates, is an important issue for their applications [1-4].

1.3 Polymer-mediated synthesis

1.3.1 Polyethyleneimine (PEI)

Polyethyleneimine (PEI), a typical water-soluble polyamine, has a large quantity of nitrogen atoms from amino groups on the linear macromolecular chains [7]. The commercial PEI molecules often have branch chains and they contain primary, secondary and ternary amino groups. The majority amino groups on the macromolecular chains can be in protonize state in aqueous solution of pH<10, which indicates that the PEI is a cationic polymer electrolyte having the strong property of conferring electrons. Furthermore, PEI chains exhibit strong adsorption ability, which is one of the new chelating agents for heavy-metal ions such as Ni^{2+}, Co^{2+}, and Cu^{2+} [7-10]. However, when PEI is used as adsorbant, it has to be immobilized on supporting materials in advance to ensure the maneuverability due to its water soluble property in nature. Insoluble polymer particles, silica, and biomass have been used as supports to crosslink PEI in order to prevent its leaching during adsorption process. In contrast, its water-soluble property facilitates the penetration of PEI chains inside the complex nanostructure, which provides high density and uniform active sites for the assembly of metal precursors on the surface. More importantly, the PEI functionalization of the intrinsic hydrophobic surface can restrains the agglomeration arising from strong interactions between supporting materials, leading to good solubility in aqueous solution. Because of its combination of the above-mentioned advantages, PEI has attracted wide attention of investigators.

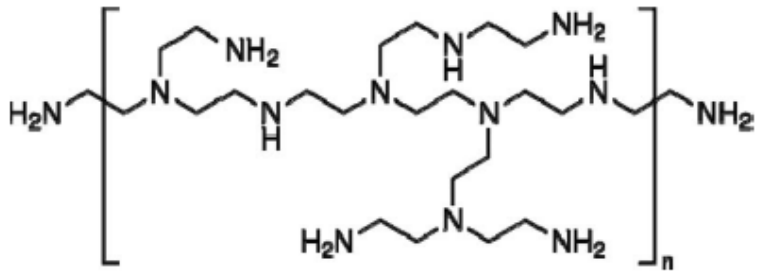

Figure 1-2. Molecular structure of PEI [11].

1.3.3 Agarose gel

The biopolymer agarose, an algal polysaccharide comprising of alternating $_{D}$-galactose and 3,6-anhydro-$_{L}$-galactopyranose repeating units, is found extensively in nature, and is often used as a model system in gelation as presented in Figure 1-3. Agarose has been widely used for food industry, pharmaceutical formulation, electrophoresis, tissue engineering, and a matrix for soft-matter organic devices due to its attractive properties of excellent film-forming ability, biocompatibility, non-toxicity, and low cost. Although agrose behaves as a semi-flexible polymer in aqueous solution at the high temperature, it can produce a gel-network through its large number of hydroxyl groups, which are formed by the presence of water molecules bound inside the double helical cavity at the low temperature. This structural property of the network including pore size within the gel can be easily controlled by altering the agarose concentration during the fabrication. Due to the facile preparation method and high stability, agarose gel has recently been reported that it may well have potential for use as a template for the synthesis of porous metal oxides by using a sol-gel method [12-14]. Furthermore, an agarose polymer matrix can be used as a mediative template for the fabrication of metal oxide thin films by electrodeposition because the polymer layer also can effectively deliver metallic precursors inside gel [15]. More importantly, during the electrodeposition process, the diffusion direction of metallic precursors can be regulated by the applied electric field through the hydrogel (Figure 1-4). In addition, agarose gel can be readily converted into a

carbonaceous matrix by carbonizing the material under a nitrogen atmosphere.

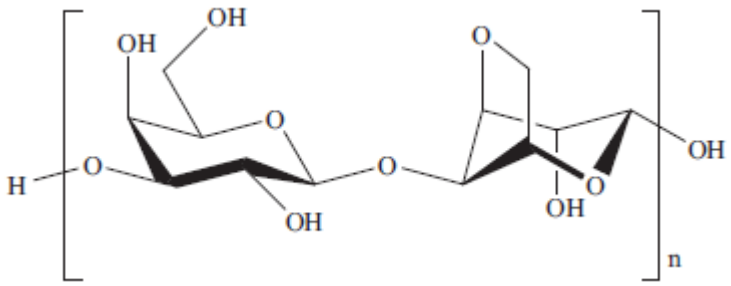

Figure 1-3. Basic repeating unit of agarose [14].

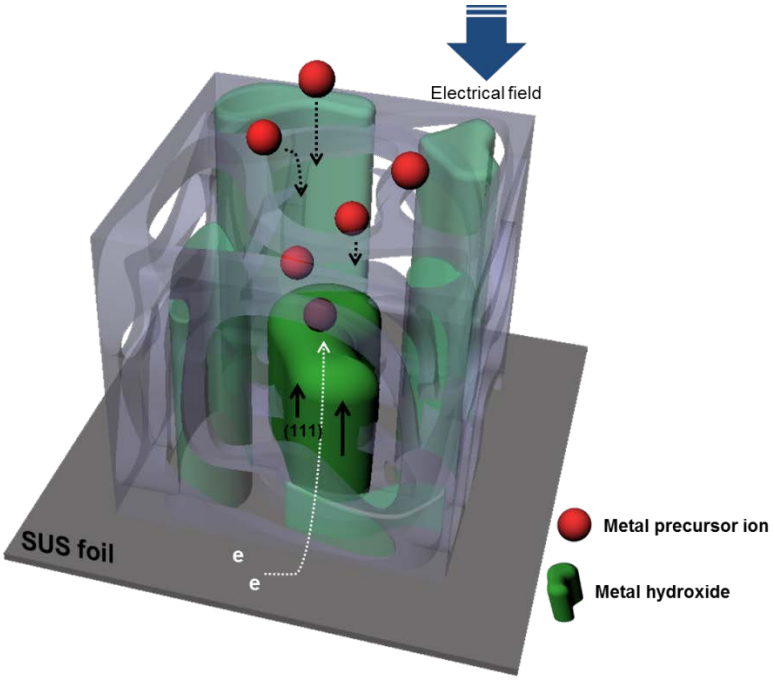

Figure 1-4. Schemetic representation of the fabrication process used for preferentially grown metal hydroxide embedded in an agarose gel.

1.4 Objectives

This thesis mainly consists of developing novel methods for fabirication of high-performance electrode materials for Li-ion battery anodes.

In the first part of this dissertation, the fabrication of nanostructured carbon/metal or metal oxide composite materials with enhanced performance via polyethyleneimine (PEI)-mediated strategy is discussed. For this purpose, firstly, graphene/metal oxide (Co_3O_4, NiO) materials with high performance and stability are prepared by co-electrodeposition. The synergistic effect of the graphene, which can assist electron transport and participate in the lithium storage process, is discussed.

In the second part of this dissertation, for the use of unique properties of agarose gel, the fabrication of preferentially grown metal oxide embedded in carbonaceous matrix is demonstrated. At first, novel method for preparation of nanostructured metal oxides (Co_3O_4, NiO) using agarose gel-mediated electrodeposition is introduced. The effect of agarose gel mediation is investigated by comparing with the normal electrodeposition method. Structural and electrochemical properties of synthesized samples are further confirmed by changing electrodeposition time.

Chapter 2. Facile preparation of graphene/metal oxide composites via polyethyleneimine-mediated strategy for Li-ion battery anodes

2.1 Synthesis of graphene/Co_3O_4 thin films for lithium ion battery anodes by co-electrodeposition

2.1.1 Introduction

Graphene with a two-dimensional structure represents a promising material for use in lithium ion batteries (LIBs) due to its superior electronic conductivity, mechanical properties, high surface area, and theoretical capacity (744 mAh/g) [16,17]. Composites based on graphene have also attracted considerable interest as electrode materials for lithium ion batteries (LIBs) [18,19]. However, the practical applications of graphene have been limited by its irreversible aggregation during the reduction process, leading to changes in intrinsic chemical and physical properties. The synthesis of graphene-metal nanocomposites was initially proposed, in an attempt to minimize the agglomeration of graphene sheets [10,20]. Although graphene-metal nanocomposites have been successfully prepared by the chemical or thermal reduction of metallic precursors in graphene oxides (GOs) dispersions, most of the currently proposed methods involve multiple steps which is very complicated.

A simple and rapid method for the direct electrodeposition of graphene-metal composites was recently developed [10,21]. Coelectrodeposited graphene-metal films are typically prepared by cyclic voltammetry because of the deposition voltage difference between graphene oxide and the metal. However, the above-mentioned method is limited to negatively charged metallic precursors because of the precipitation and agglomeration between GOs and the positively charged metal precursor. Cationic metallic precursors such as Co^{2+}, Ni^{2+} could presumably act as the cross-linkers due to their tendency to bind readily to the oxygen functional groups of GOs [8,22].

To expand this methodology to metal cationic precursors, we chemically modified GOs with poly(ethyleneimine) (PEI). Because it has been well known that PEI is an effective chelating agent due to the presence of a large number of amine groups [10-12], we expected that PEI on the surface of GOs (PEI-GOs) would provide ligand sites for complexation between the GOs and cationic precursor, which would facilitate the direct electrodeposition of the GOs/metal thin films.

The findings reported herein demonstrate the one step coelectrodeposition of a graphene/Co_3O_4 composite, which is very simple compared to previously reported methods. After heat treatment, the electrodeposited composite was employed as an anode for LIBs. We used the coelectrodeposition method for the synthesis of graphene/Co_3O_4 composite to address the following questions: (1) Can a graphene/Co_3O_4 composite be rapidly synthesized by eletrodeposition? (2) What are the roles of PEI in the electrodeposition process? (3) Does graphene improve the electrochemical

properties of cobalt oxide?

2.1.2 Experimental

2.1.2.1 Preparation of graphene/Co_3O_4 thin films

GOs were synthesized from commercially available graphite powder by a previously reported method [23]. A 0.3 g of as-synthesized GOs was dispersed in 200 ml of de-ionized (DI) water, and 0.1 g of PEI was then added to the solution. The mixed solution was stirred at 60 ^{o}C for 12 h. After cooling to room temperature, the resulting dispersion was centrifuged and washed with DI water to remove excess PEI. The resultant product was redispersed in DI water and 0.05 M of $Co(NO_3)_2$ and 0.075 M of $NaNO_3$ were added to the solution. The coelecrtodeposition was performed potentiostatically at -1.0 V (vs Ag/AgCl) for 5 min at room temperature. A stainless steel foil (SS) was used as the substrate. Prior to the deposition, the stainless steel foil (2 cm x 4 cm) was cleaned. A Pt plate and Ag/AgCl were used as the counter electrode and reference electrode, respectively. After electrodeposition, the resulting films were rinsed with DI water and dried at room temperature. The as-prepared samples were calcined at 350 ^{o}C for 2 h under a nitrogen atmosphere. Co oxides films without GOs were also prepared by a cathodic electrodeposition as a control sample.

2.1.2.2 Materials characterization

The surface morphology and composition of the electrodeposited films

were examined by scanning electron microscopy (SEM, Carl Zeiss., SUPRA 55VP) and energy dispersive spectrometer (EDS, Bruker, Xflash 5030 detector). Zeta potential was determined using zeta-potential analyzer (Otsuka, ELS-Z). X-ray photoelectron spectroscopy (XPS, Thermo, K-Alpha), and X-ray diffractometer (Rigaku, D/max-2200) were used to examine the composite structure. For the measurement of electrochemical properties, charge-discharge tests were carried out in a conventional coin cell (CR2032). A lithium foil and microporous polypropylenes were used as the negative electrode and separator, respectively. 1 M solution of LiPF6 in a mixture of ethyl carbonate (EC) and diethyl carbonate (DEC) (1:1 vol. ratio) was used as an electrolyte. Galvanostatic charge and discharge measurements were carried out with a constant current density of 700 mAg-1 in the voltage range of 0.01 ~ 3.0 V on a battery tester (WonA tech, WBCS3000). Electrochemical impedance spectroscopy was performed in a three electrode cell using a multi-potentiostat (VMP2, Princeton Applied Research).

2.1.3 Results and discussion

Typically, water-soluble PEI is reacted with GOs to be grafted onto the surface of GOs via the formation of amide bonds [22]. PEI is a cationic polymeric electrolyte that contains a large quantity of amine groups, and it can be immobilized on various surfaces due to the strong electrostatic interactions arising from these amine groups [8]. The modification of GOs surface with cationic PEI chain could result in well-dispersed GOs-based materials. Positively charged (~ 46.8 mV) PEI-GOs can be protonated in aqueous solution when pH is lower than 10 due to a large amount of nitrogen atoms [22], which can coexist with cationic metallic precursors. Because PEI has excellent adsorption property for heavy-metal ions [8], PEI grafted onto GOs could act as a kind of trapping agent for Co^{2+}, which plays a key role in sequential complexation between GOs and Co^{2+}. Thus, a synthesis of graphene/Co_3O_4 films can be achieved by cathodic electrodeposition, as shown in Figure 2-1.

SEM images of electrodeposited thin films before heat treatment are shown in Figure 2-2(a) and (b). The as-synthesized PEI-GOs/$Co(OH)_2$ thin film is comprised of a very uniform layer, and GOs appears to be well dispersed within the hierarchical structure of the electrodeposited $Co(OH)_2$. Figure 2-2(c) shows the graphene/Co_3O_4 film after calcination, and it was confirmed that the thin graphene layers are anchored on the surface of electrodeposited Co_3O_4. It should be emphasized that, in the absence of a PEI treatment, the addition of Co^{2+} ions led to agglomeration with GOs and

precipitation in the electrolyte [10]. This strongly indicates that PEI plays a significant role in the formation of uniformly dispersed films. After heat treatment, the elemental distribution of cobalt and carbon in the graphene/Co_3O_4 films was examined by EDS, shown in Figure 2-3. Both cobalt and carbon are very uniformly distributed on the electrode surface. The average ratio of carbon-cobalt is about 23.8:76.2 atomic %, respectively. The above results confirm that a graphene/Co_3O_4 composite with a very high uniformity was successfully prepared by the electrodeposition method.

The as-deposited films (after drying at room temperature) were confirmed to be amorphous (data not shown), and the XRD patterns of the electrodeposited Co_3O_4 and graphene/Co_3O_4 thin films on SS substrates after calcination at 350 ^oC are shown in Figure 2-4(a). For both films, the major diffraction lines can be assigned as Co_3O_4 (JCPDS CARD No. 42-1467). Figure 2-4(b) shows the N1s XPS spectra of coelectrodeposited graphene/Co_3O_4 films before and after calcination. As shown in Figure 2-4(b), the disappearance of the N1s peak in the XPS after the heat treatment clearly indicates that the PEI chains were completely eliminated from the resulting composite.

The electrochemical performances of the electrodeposited pure Co_3O_4 and graphene/Co_3O_4 thin films were evaluated using a coin cell. Figure 2-5(a) and (b) show the first and second charge/discharge behavior of pure Co_3O_4 and the graphene/Co_3O_4 films in the voltage range between 0.01 and 3.0 vs Li/Li^+ at 700 mA g^{-1}. As shown in Figure 2-5(a) and (b), the first discharge (1342 mAh g^{-1}) and charge capacities (1042 mAh g^{-1}) of the graphene/Co_3O_4

were much higher than those of the pure Co_3O_4 film (1209 and 899 mAh g^{-1}, respectively). In the potential range of 1.0-1.2 V, both samples show voltage plateaus that correspond to the formation of Li_2O, indicative of the typical characteristics of the voltage profile for Co_3O_4 electrodes. The cyclic performances of the two electrodes at 700 mA g^{-1} for 100 cycles are shown in Figure 2-5(c). The initial capacity drop for both cases can be attributed to the formation of a solid electrolyte interphase (SEI) layer [24]. Qian et al. reported that graphene/Co_3O_4 nanorods composites prepared by a one-spot solvothermal method exhibited much higher cycling performance than either pure graphene or pure Co_3O_4. The reversible capacity of the graphene/Co_3O_4 composites slightly increased with cycling, and maintained 1310 mAh g^{-1} at the 40th cycles, while the reversible capacity of Co_3O_4 decreased from 1184 to 85 mAh g^{-1} [25]. They concluded that the enhancement could be attributed to the synergetic effects between graphene and Co_3O_4 in terms of ion diffusion and electronic conductivity. However, the preparation method of graphene/Co_3O_4 composites involved multiple steps, which were complicated and time-consuming compared to our method. As shown in Figure 2-5(c), it is observed much enhanced cycleabilty of graphene/Co_3O_4 thin films reported herein. After 50 cycles, the capacity retention of graphene/Co_3O_4 was approximately 113 %, while the value for the pure Co_3O_4 electrode was 103 %. The capacity of the graphene/Co_3O_4 film was maintained at relatively high level up to 60 cycles (1523 mAh g^{-1}). For both electrodes, the reversible capacity anomalously increased between the 50th and 60th cycles, and then decreased rapidly. These results could be attributed

to the gradual activation by the formation of a gel-like polymeric layer within the hierarchical structure. Thereafter, the increase in the electrical resistance and isolation due to thick polymer layer results in the capacity fade [26,27]. Figure 2-5(d) displays the SEM images of graphene/Co_3O_4 electrode after 100 cycles. The hierarchical structure completely disappeared upon the conversion reaction and the formation of polymer film. From the above results, it can be concluded that uniformly distributed graphene in the film plays an important role in electrochemical lithium storage performance in Co_3O_4.

To investigate the role of the graphene as a provider of the electrical conductive network, impedance spectra were measured for both electrodes during charge-discharge (2nd and 100th cycles), shown in Figure 2-6(a) and (b). Nyquist plots for both electrodes consisted of a semicircle at high frequency, which is correlated with charge transfer resistance on the electrode interface. The Co_3O_4 thin film exhibited a much larger diameter of the semicircle compared with that of the graphene/Co_3O_4 film at 2nd cycles. Moreover, an impedance test at the end of 100 cycles indicated that Co_3O_4 without graphene shows an extremely high charge transfer resistance. From the above results, we conclude that graphene sheets serve as a conductive pathway and decreases the charge transfer resistance of Co_3O_4, resulting in an enhanced capacity and cycleability.

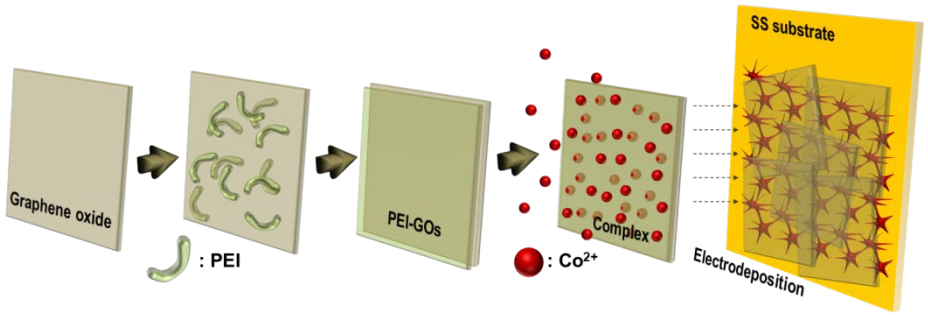

Figure 2-1. Schematic representation of the fabrication process for preparing PEI-GOs/$Co(OH)_2$ films by co-electrodeposition.

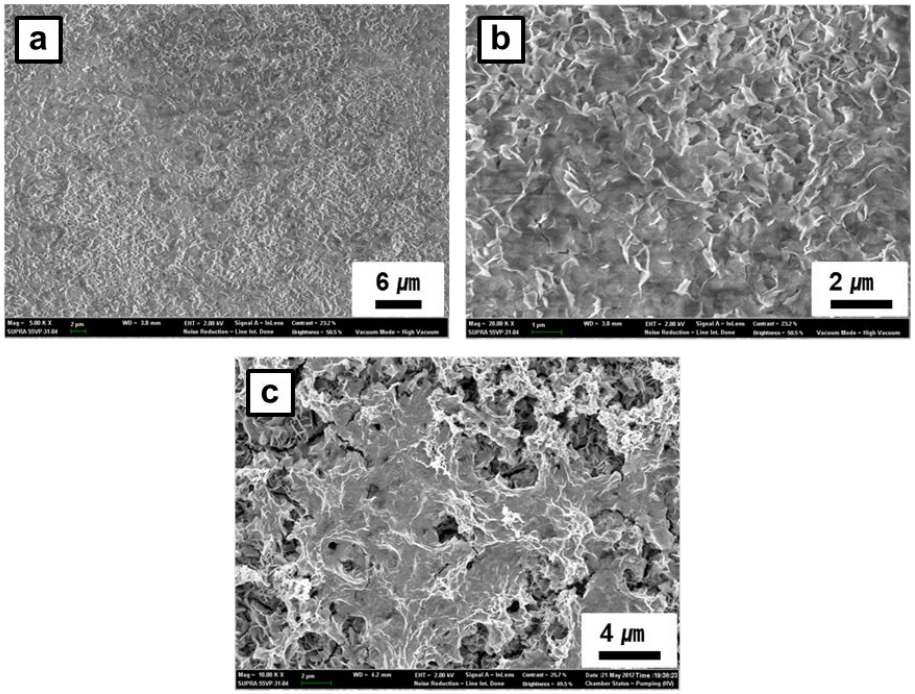

Figure 2-2. SEM images of electrodeposited thin films; (a and b) PEI-GOs/$Co(OH)_2$ and (c) graphene/Co_3O_4.

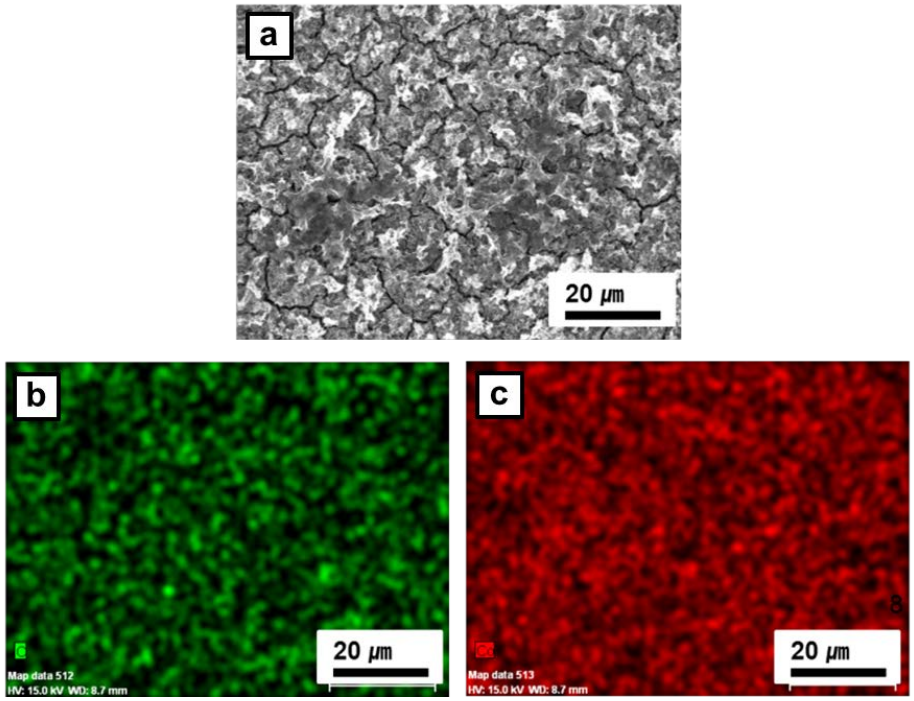

Figure 2-3. EDS atomic analysis results of graphene/Co_3O_4 film; (a) SEM images of thin film, (b) carbon, and (c) cobalt.

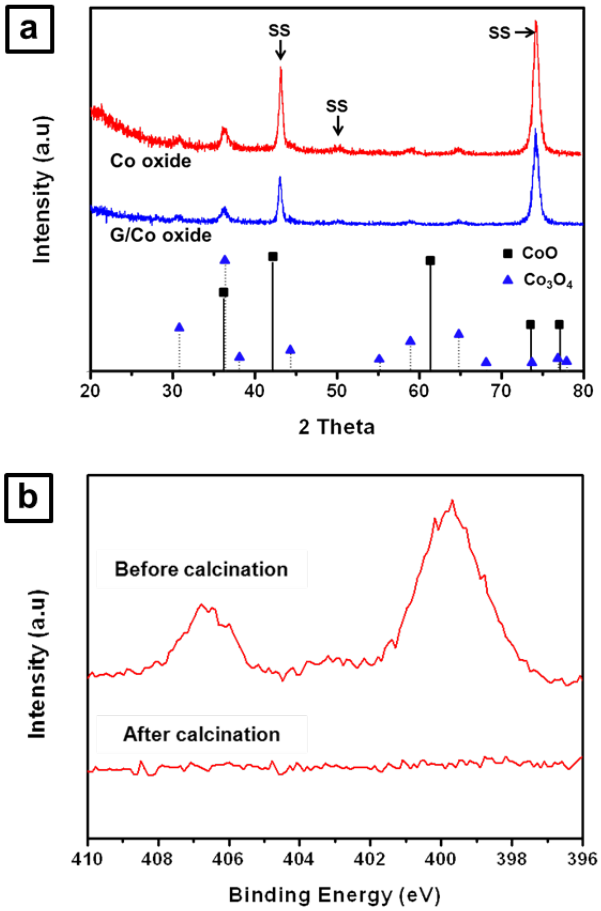

Figure 2-4. XRD spectra of Co oxide and graphene/Co oxide thin films and (b) XPS N1s spectra of graphene/Co thin films before and after calcination at 350 ^{o}C.

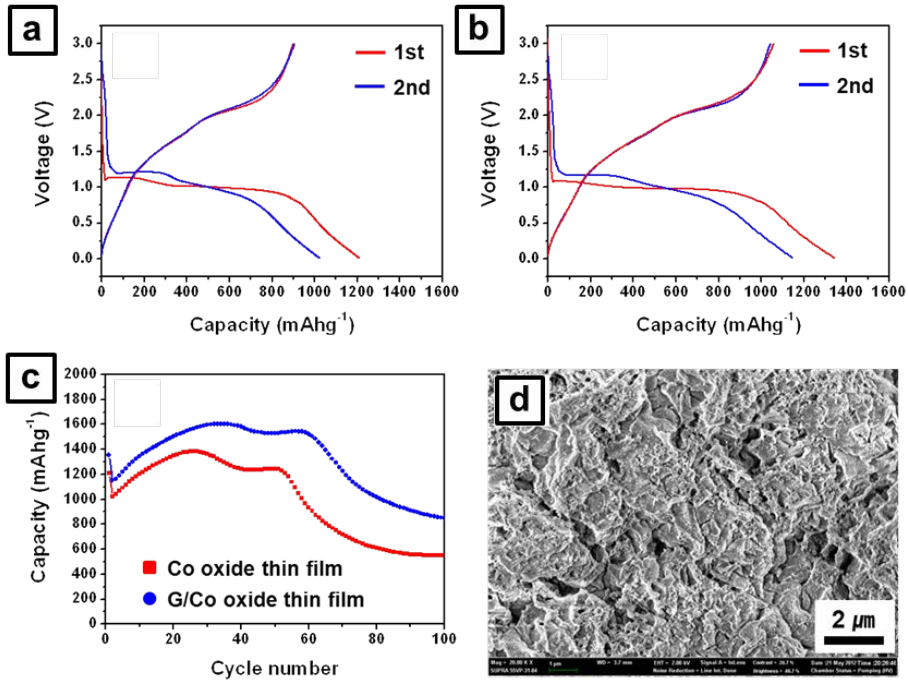

Figure 2-5. Electrochemical performance test of synthesized films; charge/discharge curves of (a) Co_3O_4 and (b) graphene/Co_3O_4, and (c) cycling performances of Co_3O_4 and graphene/Co_3O_4 thin films. (d) SEM image of graphene/Co_3O_4 electrode after 100 cycles.

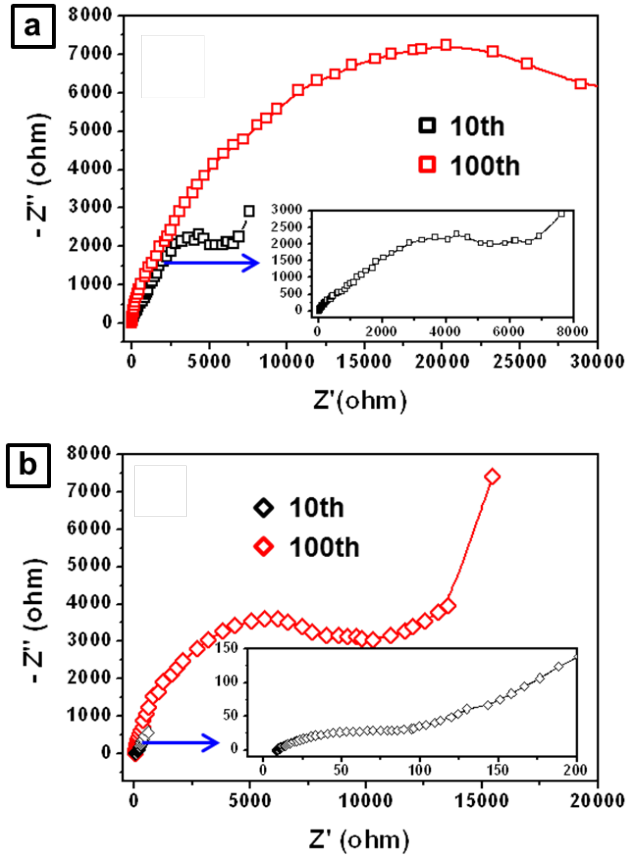

Figure 2-6. Impedance spectra of (a) Co_3O_4 and (b) graphene/Co_3O_4.

2.2 Preparation via an electrochemical method of graphene films coated on both sides with NiO nanoparticles for use as Li-ion battery anodes

2.2.1 Introduction

Due to the superior electronic conductivity, structural flexibility, and chemical stability, graphene, a new type of two-dimensional carbon material, represents an advanced material that promises to find use in lithium ion batteries (LIBs) [28-30]. However, the irreversible aggregation and restacking of graphene sheets, which lead to changes in its intrinsic chemical and physical properties during the reduction process, are problems that limit its practical applications [31,32]. To circumvent this problem, graphene-based composite materials, including transition metal oxides such as SnO_2 [30], Co_3O_4 [18], NiO [33] and Fe_2O_3 [34] have been exploited for use as anode materials for LIBs. The incorporation of metal oxides into graphene layers could reduce the degree of stacking of graphene sheets as well as to generate electron-conducting and ion-transporting pathways [34-36]. In addition, the excellent flexibility of graphene can efficiently buffer the volume expansion associated with the Li charge/discharge process [35-37]. Graphene/metal oxide composites are typically prepared by the thermal or chemical reduction of graphene oxide (GO) and metallic precursors [18,33,34]. However, the above-mentioned methods obviously involve highly toxic chemicals or high temperatures and, moreover, multiple steps

are required. Consequently, a more efficient process that includes a shorter processing time and a simplified setup for production is needed.

Electrodeposition is an effective technique that is used for the synthesis of metal oxide thin films, in which the thickness, density, and morphology can be easily controlled by adjusting the applied current, bath chemistry, and temperature [38-40]. Such an electrochemical method has recently been used for the synthesis of graphene and graphene-based metal oxide films, and has been found to be a simple and easily used tool [41-43]. However, most of the currently proposed methods typically involve two steps. A graphene oxide (GO) textile electrode is first prepared by a coating process such as dip-coating, drop-casting, or spray-coating methods. This is followed by an electrochemical synthesis with a metallic precursor that is achieved by simply dipping graphene textile into a precursor solution and subsequently performing an electrodeposition. As a result, metal oxide nanoparticles are mostly located on the surface of the graphene textile electrode, resulting in an increase in the degree of stacking of graphene sheets [41-45]. More importantly, in the case of the coelectrodeposition of graphene/metal composite, it is necessary to use negatively charged metallic precursors [10,46]. The cationic metallic precursors could presumably act as cross-linkers due to their tendency to bind readily to the oxygen functional groups of GOs, leading to the precipitation and agglomeration of GOs in the solution [10,21]. To address such critical problems, our previous work demonstrated that the modification of GOs by treatment with poly(ethyleneimine) (PEI) is a reliable method for coexisting and chelating

with positively charged metallic precursors, and also makes it possible to simultaneously synthesize graphene/metal oxide thin films [47]

Graphene/NiO is one of the promising anode materials for use in LIBs due to their extra high capacity compared to pristine graphene and NiO electrodes [33,48]. However, like other conversion-based anode materials, its practical application to LIBs is greatly restrained by detrimental effects related to its structural and electrochemical properties upon cycling because of the non-intimate contact between graphene layers and NiO nanoparticles, which would lead to a loss of electrical contact and subsequent capacity fading. In addition, the process of fabricating electrodes continues to be both time and labor intensive. Herein, we report on attempts to expand our previously reported coelectrodeposition methodology by using PEI-modified GOs (PEI-GOs). The developed method is very simple compared to previously reported methods for the synthesis of NiO/graphene films. Due to the strong formation property of PEI/Ni^{2+} complexes with a high stability [23], the complexation of PEI-GOs and Ni^{2+} ions would effectively permit migration to the substrate, which could subsequently permit the interconnected NiO nanoparticles to be coated on both sides of the graphene surface during the electrodeposition procedure. The as-synthesized material efficiently utilizes the combined merits of NiO and graphene, resulting in a product with superior performance with a large reversible capacity, excellent cycling stability, and enhanced conductivity.

2.2.2 Experimental

2.2.2.1 Preparation of PEI-modified graphene oxide

The GOs were initially synthesized by chemical exfoliation of commercially available graphite powder by a previously reported method [22]. First, 0.3 g of GOs was dispersed in 200 ml of de-ionized (DI) water by sonication for 1 h, and then transferred into a three-necked round-bottom flask. A 0.1 g of PEI was added to the above solution and then stirred at 60 ^{o}C for 12 h to ensure complete reaction. After cooling to room temperature, the obtained dispersion was centrifuged (15000 rpm for 30 min) and washed with DI water three times to remove excess PEI.

2.2.2.2 Electrodeposition of graphene/NiO composites film

The electrodeposition was performed at room temperature by a WPG100 electrochemical workstation (WonAtech) using a three-electrode system. A clean stainless steel foil (SS) was used as the working electrode. A Pt plate and Ag/AgCl were used as the counter electrode and reference electrode, respectively. The PEI-GOs was redispersed in DI water and 0.05 M of $Ni(NO_3)_2$ and 0.075 M of $NaNO_3$ were added to the solution. The coelecrtodeposition was performed potentiostatically at -1.0 V (vs Ag/AgCl) for 300 s. Afterwards, the resulting films were rinsed with DI water to eliminate residual solvents, and then dried at room temperature for 6 h.

Finally, the samples were annealed at 350 ^{o}C for 2 h under a nitrogen atmosphere. For the sake of comparison, we synthesized a pure NiO film by the same procedure without PEI-GOs for 300 s.

2.2.2.3 Materials characterization

The graphene/NiO composites were characterized by scanning electron microscopy (SEM, Carl Zeiss., SUPRA 55VP), energy dispersive spectrometer (EDS, Bruker, Xflash5030 detector), zeta-potential analyzer (Otsuka, ELS-Z), X-ray photoelectron spectroscopy (XPS, Thermo, K-Alpha), and X-ray diffractometer (XRD, Rigaku, D/max-2200). Electrochemical characterization was performed on a battery tester (WonA tech, WBCS3000) and an electrochemical workstation (WonA tech, ZIVE SP2) using a conventional coin cell (CR2032) assembled in an argon-filled glove box. A lithium foil and microporous polypropylenes were used as the negative electrode and separator, respectively. 1 M solution of $LiPF_6$ in a mixture of ethyl carbonate and diethyl carbonate (1:1 vol. ratio) was used as an electrolyte. The electrode capacity was measured by the galvanostatic charge and discharge method with a constant current density of 355 mA g^{-1} in the voltage range of 0.01-3.0 V. The frequency of EIS ranged from 0.01 Hz to 200 kHz at the open circuit potential.

2.2.3 Results and discussion

Figure 2-7 illustrates the synthetic procedure used to prepare a PEI-GOs/$Ni(OH)_2$ film by coelectrodeposition. Typically, individual GO sheets can be easily crosslinked in the presence of cationic metal precursors such as Ni^{2+} and Co^{2+}, leading to agglomeration and precipitation of the GOs [10,21]. In order to address this problem, GOs is chemically modified in the presence of PEI as a stabilizer. Because the water-soluble PEI is covalently linked to the GO sheet by the formation of amide bonds, it can be immobilized on the surface of GOs, resulting in well dispersed positively charged (~48.3 mV) GOs-based materials. In addition, molecules of PEI containing amino and imino groups enable stable chelates with transition metal ions to be formed [47,49]. Consequently, PEI-GOs can not only coexist with cationic metallic precursors but also can play a key role in sequential complexation between GOs and Ni^{2+}. When the PEI-GOs/Ni^{2+} complex arrives at the SS substrate, electrochemical reduction of the GOs can occur under cathodic conditions, which allows electrons to be conducted to the outer layer of the graphene sheet [43-45]. As a result, the nickel ions chelated at the surface of PEI-GOs are easily converted into $Ni(OH)_2$ on the surface of the GOs. The hydroxide ion (OH^-) is produced by the reduction of NO^{3-} under cathodic condition. The generation of OH^- close to the cathode increases the local pH, resulting in the precipitation of $Ni(OH)_2$. The $Ni(OH)_2$ continues to deposit through the transport of freely moving Ni^{2+} ions in the solution. Afterwards, the PEI-GOs/$Ni(OH)_2$ film is subsequently converted into graphene/NiO by

calcination at 350 ^{o}C under a nitrogen atmosphere. Thus, the synthesis of graphene/NiO can be achieved by coelectrodeposition.

The morphology of the as-synthesized films was studied by TEM as shown in Figure 2-8. Figure 2-8(a) and (b) show the as-prepared PEI-GOs/$Ni(OH)_2$ thin film before the heat treatment, from which it can be clearly seen that the $Ni(OH)_2$ films are directly deposited on the thin GO layer. After annealing at 350 ^{o}C for 2 h, the interconnected NiO nanoparticles are uniformly coated on graphene sheets (Figure 2-8(c) and (d)). The existence of GO and graphene can be determined by the graphene structure with thin layers observed on the edge of the samples (arrow area in Figure 2-8(b) and (d)).

The SEM images of electrodeposited thin films before and after the heat treatment are shown Figure 2-9. The electrodeposited $Ni(OH)_2$ film without GOs has a homogeneous dense structure which is comprised of large grains representing aggregates of small nanoscale-sized particles (Figure 2-9(a) and (b)). In the case of the PEI-GOs/$Ni(OH)_2$, the as-prepared thin film appear to be well deposited on the substrate surface, resulting in the uniform coating of loosely packed $Ni(OH)_2$ nanoparticles network on the GOs (Figure 2-9(c)). The formation of hierarchical morphology of $Ni(OH)_2$ nanoparticles is clearly observed. Figure 2-9(d), which shows the graphene/NiO film after calcination, confirms that the interconnected NiO nanoparticles are strongly anchored to the graphene sheets. Due to high-density deposited NiO, the graphene is not seen directly in the images. The above results strongly indicate that the PEI treatment plays a significant role in the

coelectrodeposition process, when cationic metallic precursors are used. In addition, NiO nanoparticles coating layer acts as spacers on both sides of graphene surface, effectively preventing the aggregation and restacking of graphene sheets upon cycling. Consequently, this favorable structure could permit a large electrode/electrolyte contact area to be maintained.

To further confirm the distribution of graphene nanosheets, EDS mapping was employed (Figure 2-10). The SEM image in Figure 2-10(a) indicates that a thin layer of graphene/NiO is homogeneously deposited on the substrate. The corresponding elemental mapping of Ni (Figure 2-10(b)) and carbon (Figure 2-10(c)) displays that both the nickel oxide and graphene are distributed uniformly on the electrode surface. From the above result, a graphene/NiO thin film with a high uniformity is successfully synthesized by coelectrodeposition. In addition, it can be concluded that the PEI-GOs/Ni^{2+} complex would efficiently migrate to the SS substrate under the applied electric field. Moreover, well-distributed graphene sheets would play an important role as a conductive network within the deposited layers, leading to enhanced electrochemical performance.

The as-deposited films (after drying at room temperature) were confirmed to be amorphous (data not shown). Figure 2-11 displays XRD diffraction patterns for the electrodeposited NiO and graphene/NiO thin films on a stainless steel substrate after calcination at 350 ^{o}C under a nitrogen atmosphere. For both films, the main diffraction lines at 37.2, 43.3, and 62.8^{o} correspond to (111), (200), and (220) crystalline of cubic NiO phase (JCPDS 47-1049), respectively [50]. This result clearly indicates that the deposited

$Ni(OH)_2$ is converted into nickel oxide as the result of the heat treatment. For the graphene/NiO thin film, the diffraction peak of graphene was not observed because the relatively small amount of graphene component compared to that of NiO could be electrodeposited. The existence of graphene was confirmed by EDS (see Figure 2-10(c)). Furthermore, the graphene content was determined to be approximately 12.7 wt%, from TGA measurement (data not shown).

XPS spectra of coelectrodeposited graphene/NiO films before and after calcination are shown in Figure 2-12. As shown in Figure 2-12(a), the appearance of a N1s peak before the heat treatment clearly indicates that the PEI chains were absorbed onto the GOs. In addition, the N1s spectrum of electrodeposited PEI-GOs/$Ni(OH)_2$ before calcination shows pronounced peaks at 400.6 and 399.4 eV, corresponding to $–NH_2$ and –NH–C=O functionalities, respectively (Figure 2-12(b)) [49,51]. Because the PEI chains contain large numbers of $–NH_2$ groups, it is reasonable to assume that the PEI would be grafted onto the surface of GOs by the formation of amide bonds. Furthermore, the XPS spectrum of a coelectrodeposited film after calcination confirms that the PEI chains are completely eliminated from the resulting graphene/NiO film (Figure 2-12(a) and (b)) [47].

The electrochemical performances of the electrodeposited pure NiO and graphene/NiO thin films were evaluated using a standard coin cell. Figure 2-13(a) and (b) show the initial two charge-discharge curves for the pure NiO and graphene/NiO electrodes, measured between 0.01 and 3.0 V at a rate of 0.5 C (1 C = 718 mAh g^{-1}). The specific capacities were calculated based on

the total mass of the deposited active materials. The first discharge and charge capacities are 992 and 543 mAh g^{-1} for the pure NiO, corresponding to an initial columbic efficiency of 54.7% (Figure 2-13(a)). By contrast, a large discharge capacity of 1272 mAh g^{-1} and a reversible capacity of 754 mAh g^{-1} are achieved for graphene/NiO thin film, corresponding to an improved initial columbic efficiency of 59.3% (Figure 2-13(b)). Although a long voltage plateau is found around 0.5 V for the both samples, which is contributed to the reduction of NiO to Ni and the formation of solid electrolyte interface (SEI) film, potential region lower than 0.5 V corresponding to the lithium intercalation into the graphene sheet is not visible for NiO film [52]. It is apparent that uniformly distributed graphene between NiO nanoparticles clearly has a synergetic effect. The initial capacity drop could be large due to the formation of SEI film on the surface of the active materials, the electrolyte decomposition, and the electrochemical reduction of residual oxygen-containing functional groups on graphene surface with lithium ions [33,52,53]. Figure 2-13(c) shows the cyclic performances of the pure NiO and graphene/NiO films at a current density of 0.5 C between 0.01 and 3.0 V. The reversible capacity of the graphene/NiO electrode is maintained at relatively high level up to 50 cycles (586 mAh g^{-1}), which is 78% retention of the initial charge capacity. The pure NiO film shows a reversible capacity of 198 mAh g^{-1} after 50 cycles, just 36% of the initial charge capacity. In addition, the graphene/NiO electrode exhibits an extra discharge capacity until 45 cycles (Figure 2-13(c)). This result can be attributed to gradual activation within the structure

of NiO deposited on both sides of the graphene sheet. After that, the structure appeared to reach a stabilized state. The rate capabilities of both electrodes were also investigated at various rates from 0.5 C to 2 C (Figure 2-13(d)). It is obvious that the current density has little impact on reversible capacity. However, the capacity of the NiO dropped more rapidly than that of the graphene/NiO. More importantly, when the rate returns to the initial 0.5 C after 40 cycles, the graphene/NiO electrode delivers a discharge capacity of 502 mAh g^{-1}, whereas, in the case of bare NiO, only 234 mAh g^{-1} reversible capacity is observed. From the above results, the improved electrochemical performance of the graphene/NiO thin film for lithium storage could be reasonably attributed to the synergetic effects of graphene and interconnected NiO nanoparticles. The NiO nanoparticles play a key role in the effective separation and stabilization of graphene sheets, which prevent a loss of unique intrinsic properties of graphene. Hence, the graphene not only contributed to the overall capacity but also prevent the aggregation of active materials.

In order to further elucidate the effect of graphene as a provider of an electrical conductive network, impedance spectra were conducted on the pure NiO and graphene/NiO electrodes during charge-discharge (2nd and 50th cycles), and the results are shown in figure 8. Apparently, the diameter of the semicircle for the graphene/NiO electrode is somewhat small with respect to that of the pure NiO film at the 2nd cycle, indicating the smaller surface resistance and charge transfer resistance [47,52]. Thereafter, the impedance test at the end of 50 cycles indicated that NiO without graphene

shows an increased charge transfer resistance (figure 2-14(a)). It is possible that lithium-ion conduction inside the SEI layers and charge transfer at the electrode/electrolyte interface is hindered by the increase in internal defects and isolated active regions due to the volume change and subsequent microstructural failure during continued cycling [52,54,55]. In contrast, the semicircle, corresponding to the graphene/NiO film, shows extremely low charge transfer resistance after 50 cycles (Figure 2-14(b)). This behavior indicates that the NiO nanoparticles deposited on the graphene surface are favorable for the formation of thicker SEI film [55]. The graphene/NiO structure appears to reach a stabilized state, which is consistent with the observed extra capacity of graphene/NiO electrode for up to 45 cycles (figure 2-13(c)). In addition, to confirm the structure integrity of the as-synthesized films, the evolution of the morphology and structure of NiO and graphene/NiO were investigated after 50 cycles, as shown in Figure 2-15. The SEM image of the NiO film clearly shows that the deposited NiO suffers from severe cracking and subsequently deteriorates with the film being peeled off from the substrate (Figure 2-15(a)). In contrast, the graphene/NiO retains its structural integrity with only a slight deformation (Figure 2-15(b)). The above results are consistent with the development of a synergistic effect as the result of the NiO deposited on graphene, which leads to an improved electrochemical performance. The highly conductive graphene and interconnected NiO nanoparticles facilitate continuous conductive pathways for electrons and provides a sufficient electrolyte contact area, resulting in the formation of a stable SEI layer. Moreover, the

unique structure of the electrodeposited graphene/NiO film can effectively maintain the structural integrity by accommodating the pulverization of active materials during the cycling process.

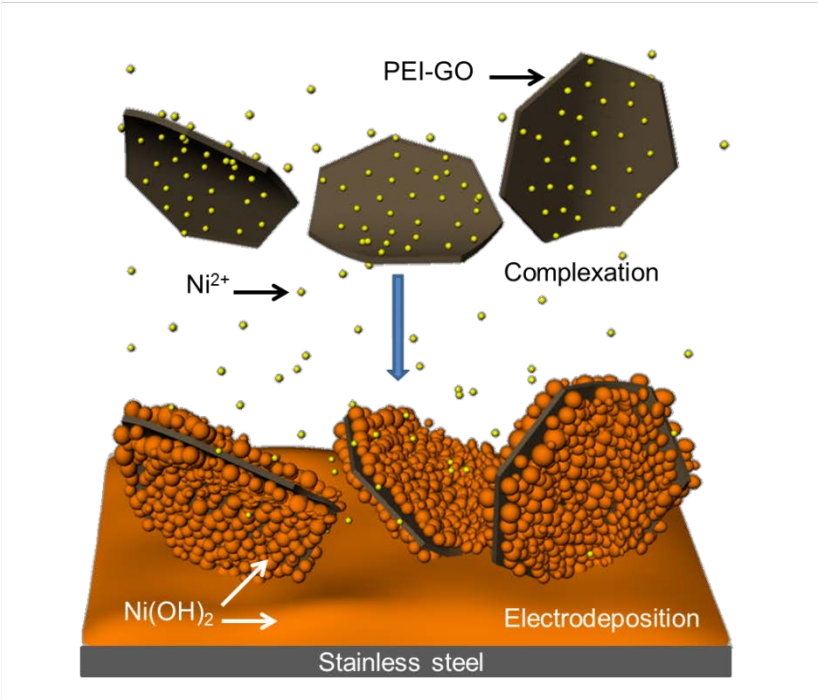

Figure 2-7. Schematic representation of the fabrication process used for prepareing PEI-GO/$Ni(OH)_2$ films by co-electrodeposition.

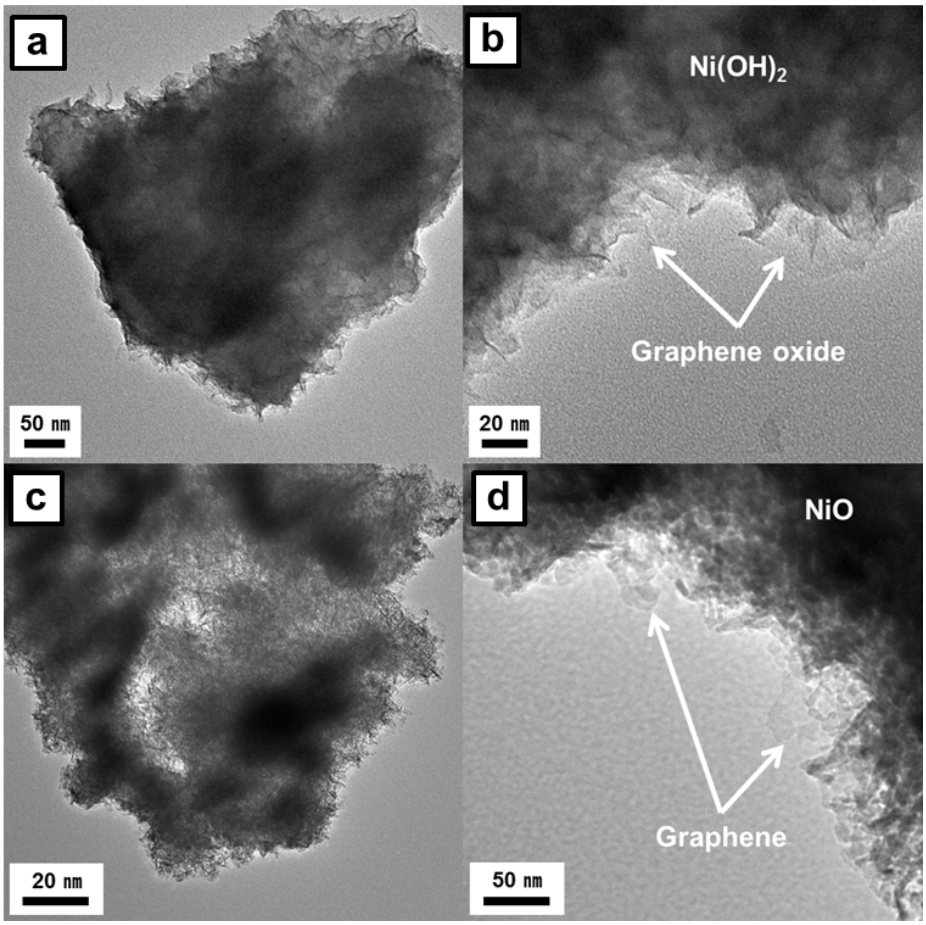

Figure 2-8. TEM images of electrodeposited thin films: (a and b) PEI-GO/$Ni(OH)_2$ and (c and d) graphene/NiO.

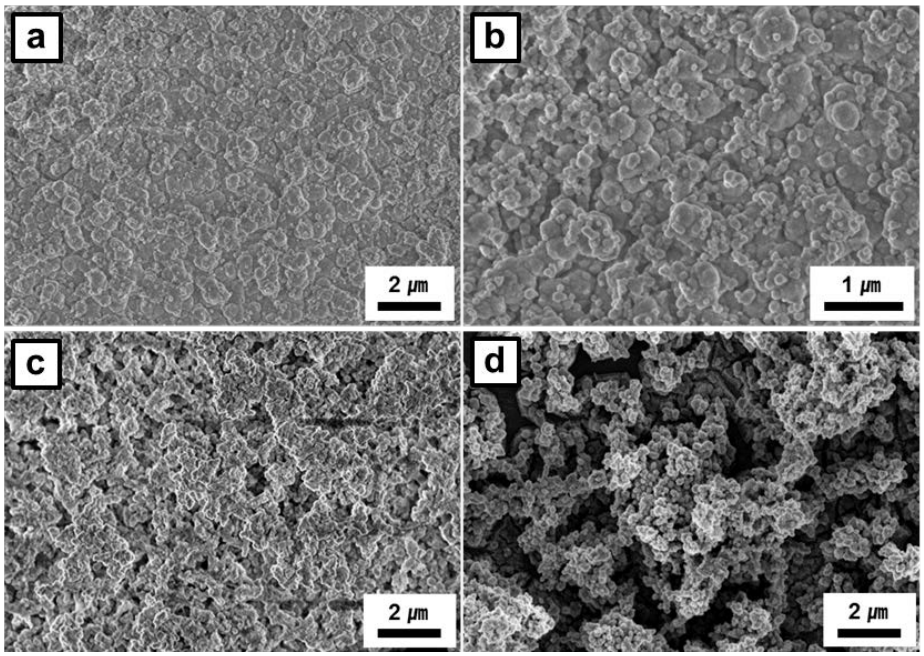

Figure 2-9. SEM images of electrodeposited thin films: (a and b) $Ni(OH)_2$, (c) PEI-GO/ $Ni(OH)_2$, (d) graphene/NiO.

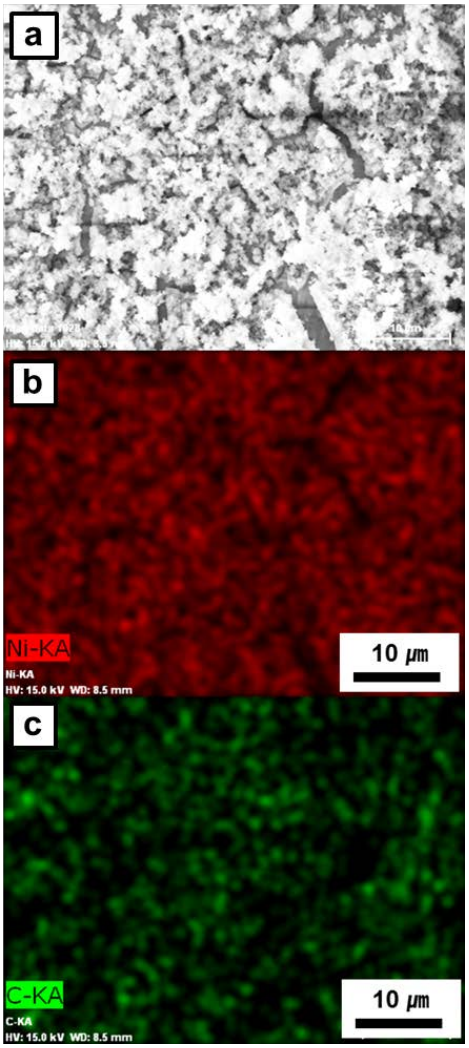

Figure 2-10. EDS atomic analysis results of graphene/NiO film: (a) SEM image of thin film, (b) nickel, and (c) carbon.

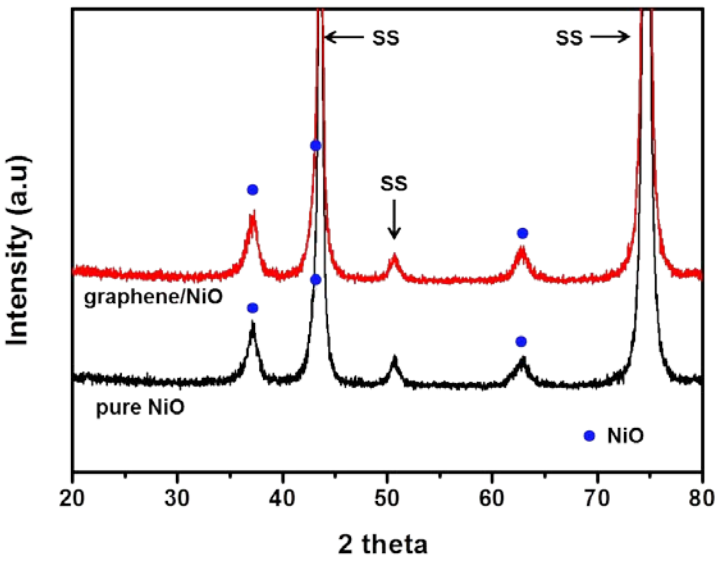

Figure 2-11. XRD spectra of NiO and graphene/NiO thin films after calcination at 350 ^{o}C.

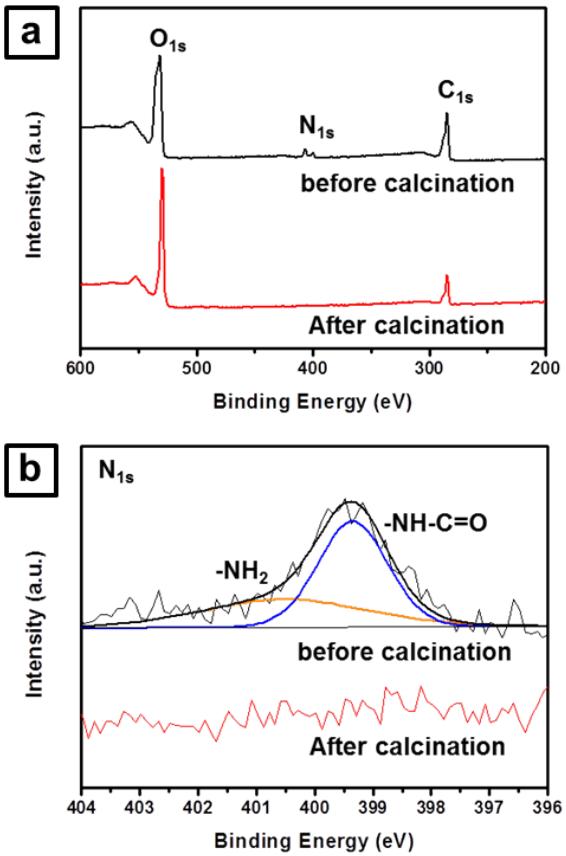

Figure 2-12. XPS spectra of graphene/NiO thin films before and after calcination. (a) Wide scan survey spectra and (b) XPS N 1s spectrum of as-synthesized films.

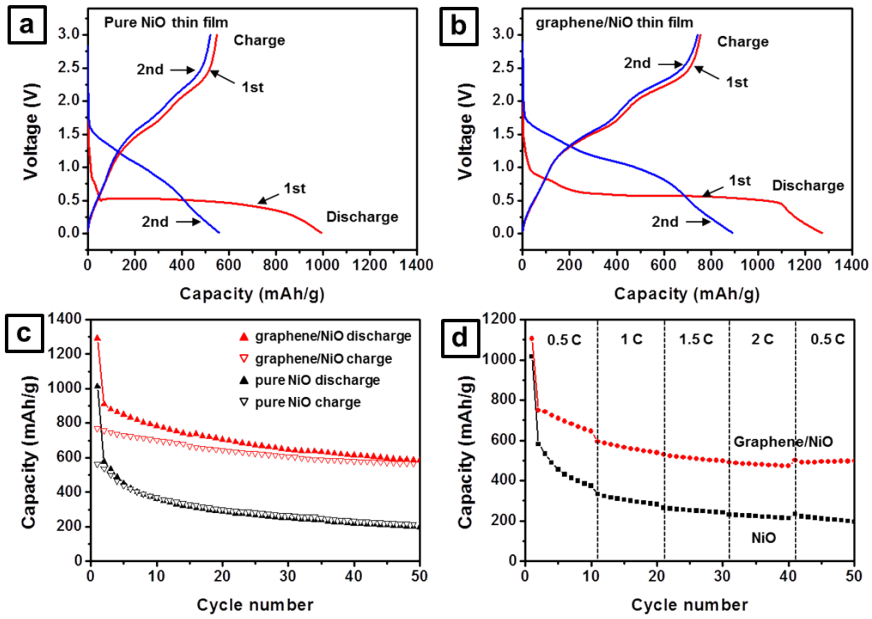

Figure 2-13. Electrochemical performance test of electrodeposited films: charge/discharge curves of (a) NiO film and (b) graphene/NiO film, (c) cyclability of NiO and graphene/NiO films with a current density of 359 mA h g^{-1} (0.5 C), and (d) rate capability test of NiO and graphene/NiO films.

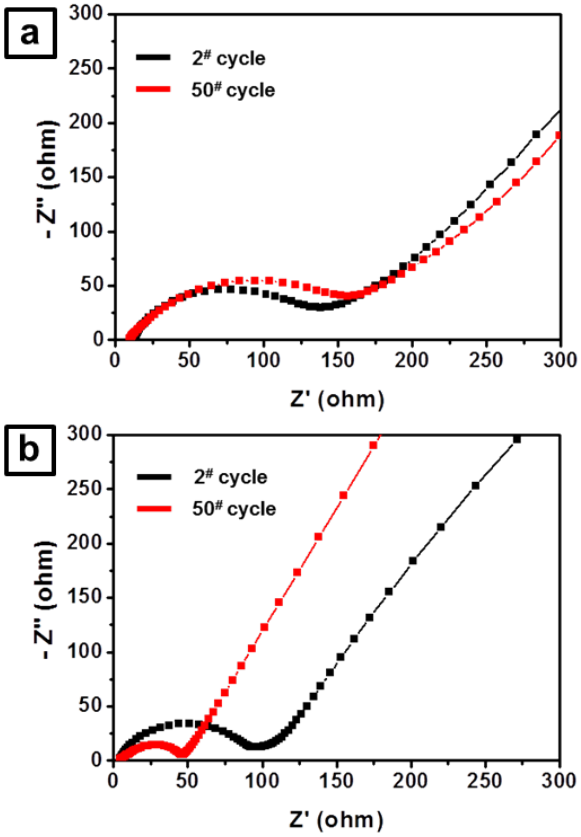

Figure 2-14. Impedance comparison curves: (a) NiO films and (b) graphene/NiO film.

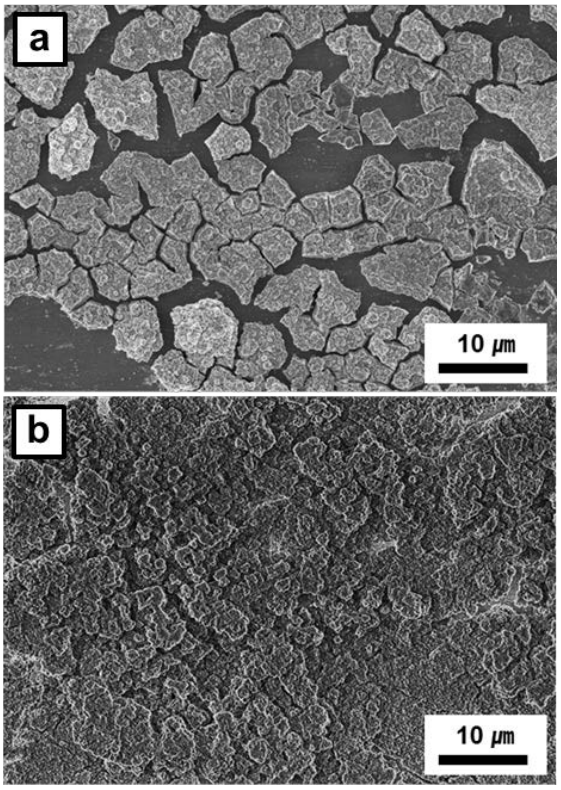

Figure 2-15. SEM images of electrodes after 100 cycles: (a) NiO and (b) graphene/NiO.

Chapter 3. Preferential growth of metal oxides via agarose gel-mediated electrodeposition for Li-ion battery anodes

3.1 Agarose gel-mediated electrodeposition: Preferential growth of Co_3O_4 anode material for lithium-ion batteries

3.1.1 Introduction

Agarose, a naturally occurring polysaccharide, is widely used in the production of various food products and in biological research [13,56]. Gelated agarose, with sub-micrometer pores, have strong elasticity, environmental benignness, and low cost, which allows such materials to be used in a variety of applications in different areas [57-59]. Furthermore, the agarose polymer matrix can be used as a meditative template for the fabrication of metal-based thin films by electrodeposition because the thin polymer layer not only has excellent film-forming characteristics on the substrate and a high stability in an aqueous solution but also can effectively deliver metallic precursors inside the gel [60,61]. In addition, the polymer gel can be converted into a carbonaceous matrix by a carbonization [62]. More importantly, during the electrodeposition process, the direction of diffusion of the metallic precursors can be regulated by an applied electric field through the hydrogel, which would be the dominant factor for

anisotropic crystal growth [63]. Taking advantage of the above-mentioned properties, we fabricated a preferentially oriented structure of metal oxide embedded in a carbonaceous matrix for high performance lithium-ion batteries (LIBs). Our concept efficiently utilizes the combinative merits of the preferential growth and heterogeneous hybridization simultaneously via 'agarose gel-mediated electro-deposition'.

Co_3O_4 has attracted considerable interest as a possible substitute for anodes that contain conventional carbonaceous materials, due to its high theoretical capacity (890 mAh g^{-1}), which would be expected to meet the requirements for energy storage systems [64,65]. However, the huge volume expansion that occurs during cycles and the formation of polymeric substances on the surface associated with the conversion reaction causes a loss of electrical connectivity and severe electrical isolation. This overall process results in rapid capacity fading and poor cycling stability [66,67]. To solve these intractable problems, various methodologies have been developed to mitigate the pulverization and further enhance the structural stability of Co_3O_4 materials, such as nanotubes [65,68], nanoflowers [69], nanowires [66], nanorods [70], and the use of carbon-based composites to produce different architectures.[71,72] Although remarkable achievements have been made, maintaining a large reversible capacity, high electrical conductivity, and long cycling stability continue to be a challenging issue.

The findings reported herein demonstrate the use of agarose-mediated electrodeposition as a strategy for the synthesis of preferentially grown Co_3O_4 embedded in a conducting carbonaceous matrix (Co_3O_4/C). The as-

synthesized composite was employed as an anode for LIBs. We used the agarose gel-mediated electrodeposition method for the synthesis of Co_3O_4/C composite to address the following questions: (1) Can a preferentially grown Co_3O_4/C film be rapidly synthesized by electrodeposition? (2) What is the role of the agarose gel in the electrodeposition process? (3) Does a preferentially oriented Co_3O_4 structure embedded in a carbonaceous matrix improve electrochemical properties?

3.1.2 Experimental

3.1.2.1 Preparation of preferentially grown Co_3O_4 embedded in a carbonaceous matrix

The agarose gel was initially prepared by dissolving powdered agarose (1 g) in deionized (DI) water (99 mL) with vigorous stirring at room temperature. The solution was heated to boiling using a microwave oven. The above aqueous solution was then cast on stainless steel (SS) substrates (2 x 3 cm) by a dip-coating method, followed by gelation and drying at room temperature for 4 hours. 0.05 M of $Co(NO_3)_2$ and 0.075 M of $NaNO_3$ were added to the DI water. The electrodeposition was performed potentiostatically at – 1.0 V (vs Ag/AgCl) for various times (100, 200, 300, 400 s) at room temperature. The agarose coated SS was employed as a working electrode. A Pt plate and Ag/AgCl were used as the counter electrode and reference electrode, respectively. After electrodeposition, the as synthesized films were rinsed with DI water and dried at room temperature for 24 h. The resulting films were calcined at 350 ^oC for 2 h under a nitrogen atmosphere. For comparison, a pure Co_3O_4 film without an agarose template was electrodeposited following the similar procedure without an agarose template for 300 s.

3.1.2.2 Materials characterization

The surface morphology and composition of the electrodeposited films were obtained by scanning electron microscope (SEM, Carl Zeiss, SUPRA 55VP), focused-ion beam microscope (FIB, Carl Zeiss, AURIGA), and energy dispersive spectrometer (EDS, Bruker, Xflash5030 detector). X-ray diffraction (XRD, Rigaku, D/max-2200) was used to examine the composite structure. Chemical bonding information was studied with fourier transform infrared spectroscope (FT-IR, Thermo Scientific, Nicolet 6700).

3.1.2.3 Electrochemical measurement

Electrochemical experiments were performed using a conventional coin cell (CR2032) assembled in an argon-filled glove box. A lithium foil and microporous polypropylenes were used as the counter electrode and separator, respectively. The electrolyte solution was a solution of 1 M $LiPF_6$ in a mixture of ethyl carbonate and diethyl carbonate with the volume ratio of EC/DEC = 1:1. The electrode capacity was measured by the galvanostatic charge and discharge method with a constant current density of 890 mA g^{-1} in the voltage range of 0.01-3.0 V on a battery tester (WonA tech, WBCS3000). The electrochemical impedance spectroscope (EIS) of the electrode was performed on an electrochemical workstation (WonA tech, ZIVE SP2). The frequency of EIS ranged from 0.01 Hz to 200 kHz at the open circuit potential.

3.1.3 Results and discussion

Figure 3-1 illustrates the synthetic procedure of preferentially grown Co_3O_4/C by agarose-mediated electrodeposition. First, the stainless steel (SS) substrate was immersed in a heated agarose solution. On cooling, a water filled gel was formed by the hydroxyl groups, which is an attractive space that exhibits a 3-dimensional interconnective porous structure [56-59]. $Co(OH)_2$ was then incorporated into the agarose gel coated substrate by electrodeposition. Typically, individual Co^{2+} ions are able to freely move around in a variety of directions, resulting in a randomly porous structure composed of interconnected-nanoflakes produced by electrodeposition [47]. However, in the case of agarose-mediated electrodeposition, the agarose gel provides pathways for both electron and Co^{2+} ions [73]. The ions linearly and compulsorily migrate inside the gels because a linear electric field is applied to the substrate, which plays a key role in the preferentially oriented growth [63]. Consequently, ions that are oriented in one direction (vertical to the substrate) will be reduced, leading to the final formation of a vertically aligned $Co(OH)_2$ layer. Finally, the $Co(OH)_2$/agarose gel is subsequently converted into Co_3O_4/C by calcination at 350 ^oC under a nitrogen atmosphere. Thus, the synthesis of preferentially grown Co_3O_4/C can be achieved by agarose-mediated electrodeposition.

Cross-sectional and top view SEM images of Co_3O_4/C thin film electrodeposited for 300s (Co_3O_4/C_300s) after heat treatment are shown in Figure 3-2. The as-synthesized Co_3O_4_300s (without an agarose gel template)

exhibits a typical hierarchical structure comprised of vertically interconnected nanoflakes (Figure 3-2(a) and (b)). In the case of agarose-mediated electrodeposition (Figure 3-2(c) and (d)), the Co_3O_4 nanoflakes are homogeneously embedded in the carbon matrix. Only slight interconnected nanoflaky structures are observed on the carbon surface. Furthermore, the electrodeposited Co_3O_4 embedded in the carbon matrix shows a vertically aligned and interconnected porous structure (Figure 3-2(e)). From EDS mapping, the cobalt is very uniformly distributed on the electrode surface (Figure 3-2(f)). The effect of deposition time on the morphologies of the films was investigated. The findings are shown Figure 3-2(d), (e), and Figure 3-3. The results indicate that the agarose gel template is a key parameter for growing Co_3O_4 thin films. When the thickness of the electrodeposited Co_3O_4 is less than that of the agarose gel template, the Co_3O_4 film shows a close-packed and porous structure. However, a hierarchical interconnected structure is formed as the deposited film thickness increases to more than the thickness of agarose gel template. This result strongly indicates that agarose mediation plays an essential role in the formation of homogeneous Co_3O_4 structure. In addition, the Co and C contents of the electrodeposited films were examined by EDS (Figure 4-4). The weight percent of Co was found to increase (64.7, 71.5, 73.0, 76.3 %) with the increase of the deposition time (100, 200, 300, 400s, respectively). This result demonstrates that the cobalt content in the carbon matrix can be easily controlled by the electrodeposition time.

In order to verify the influence of agarose-mediated electrodeposition on the structural properties of Co_3O_4, we compared a bare Co_3O_4 film and

Co_3O_4/C films by X-ray diffractometry (Figure 3-5). The XRD patterns of Co_3O_4/C show an unusually strong (111) diffraction peak in comparison with that of the pure Co_3O_4 [66], indicating that anisotropic ion diffusion inside the agarose gel could be the dominant factor for the preferential orientation of the material [47]. This is a very interesting result and is entirely contrary to previous reports on the electrodeposition of Co_3O_4 that were simply grown on bare substrates such as Ni, SS [74]. In addition, the (111) reflection intensity reached a maximum, and then the intensity of the (311) reflection was increased gradually with electrodeposition time, indicating that the interconnective nanoflaky structure could be formed as the result of a gradual increase in the outward growth of $Co(OH)_2$ nanoflakes from the agarose template. It should be noted that the agarose layer has a significant effect on the crystalline phase of the electrodeposited Co_3O_4.

The chemical transformation that occurs when the agarose gel is converted into carbonaceous products via a heat treatment under a nitrogen atmosphere was examined by FT-IR spectrometry. Figure 3-6 shows that FT-IR spectra of agarose gel before and after calcination. Prior to the calcination, a broad and intense band around 3400 cm^{-1} can be attributed to –OH stretching vibrations, which results from the hydroxyl group of water and agarose. This band is correlated to the OH banding mode (1644 cm^{-1}) of water absorbed to the agarose and the peak at around 2900 cm^{-1} is attributed to a –CH stretching vibration. In contrast, the adsorption bands corresponding to the carbonaceous matrix (after calcination) exhibited peaks at 1701 and 1606 cm^{-1} corresponding to C=O and C=C vibrations, respectively. Moreover, the

decrease in the intensity of the bands at 1000-1460 cm^{-1} and the broad band at 3000-3700cm^{-1} process [75,76]. This result implies that the $Co(OH)_2$/agarose gel thin film can be readily converted into a Co_3O_4/C composite by carbonizing the film under a nitrogen environment at 350 ^oC for 2 h.

The electrochemical performances of the pure electrodeposited Co_3O_4 and Co_3O_4/C thin films were evaluated using a standard coin cell. The specific capacities were calculated based on the weight of the total active materials, including a carbonaceous matrix. Figure 3-7(a) shows the first charge/discharge curves of the Co_3O_4/C with respect to deposition time (100, 200, 300, 400 s) in a potential window of 10 mV to 3.0 V vs Li/Li^+ at 890 mA g^{-1} (1 C rate). As shown in Figure 3-7(a), similar discharge-charge behaviors were found for the four samples which had been electrodeposited using agarose mediation. The four electrodes have a specific capacity of 327, 614, 979, and 1171 mAh g^{-1} in the discharge step and a reversible capacity of 195, 488, 561, and 648 mAh g^{-1} in the charge step, respectively. The capacity difference among the four samples could be caused by the difference in the amount of cobalt oxide in the as-synthesized films. A long voltage plateau was found around 1.0 V for the pure Co_3O_4_300s electrode, which is attributed to the reduction process of Co_3O_4 and the formation of Li_2O, indicative of the typical characteristics of the voltage profile for Co_3O_4 anode materials. However, the potential regions lower than 0.9 V corresponding to the formation of the SEI layer and the Li-storage in pure Co_3O_4 and in carbonaceous matrix were not visible for Co_3O_4_300s film [47,77]. The initial capacity drop could be large due to an incomplete conversion reaction and

irreversible lithium loss due to the formation of a solid electrolyte interphase (SEI) [47]. In order to optimize the composition of Co_3O_4, the electrochemical activity of the Co_3O_4/C composites electrodeposited with various times was evaluated by monitoring cycling performance at 890 mA g^{-1} for 150 cycles, and results are shown in Figure 3-7(b). The cycling performances of the as-synthesized samples gradually increased with increasing deposition time. The Co_3O_4/C composites (100, 200, 300, 400 s) exhibited a reversible capacity of 262, 531, 625, 667 mAh g^{-1} at the 10th cycle, respectively. For all samples, the reversible capacity increased anomalously with increasing cycling numbers, which can be contributed to gradual activation by the formation of polymer/gel like film within the interconnected porous nanostructure, as shown in Figure 3-2(e) and 3-3 [26,47,69]. However, it can be seen that the reversible capacity of Co_3O_4/C electrodeposited for 400 s (Co_3O_4/C_400s) decreased slightly after 40 cycles. The reason for this is likely due to an increase in the thickness of the polymer layer within the nanoflaky network structure, which would lead to severe electrical resistance and isolation, and hence capacity fades [71]. The anodes retained a reversible capacity of 360, 739, 709, and 619 mAh g^{-1} at 150th cycle, respectively. In the case of C thin films without Co_3O_4, low level of capacities (53 mAh g^{-1} at 100th cycles) were measured. Therefore, there is no significant contribution of agarose gel-derived carbon sources to the overall capacity of as-prepared composite films during the cycling process. The rate capabilities of the Co_3O_4/C with electrodeposition time were also investigated at various rates from 0.5 C to 2 C (Figure 3-7(c)). It is obvious that the current density has little impact on the

reversible capacity. More importantly, when the rate returns to the initial 0.5 C (445 mA g^{-1}) after 40 cycles, the composite electrode recovers its original capacity (740 mAh g^{-1} for the 50th cycle). However, capacity fading for Co_3O_4/C_ 400s occurs after 47 cycles. From the above results, it can be concluded that Co_3O_4/C_300s has an optimal composition for having high electrochemical properties. Compared with pure Co_3O_4_300s anodes without a carbon matrix, the high reversibility and enhanced stability of these composites is even more strongly highlighted, as shown in Figure 3-7(d). The capacity value for Co_3O_4/C_300 has been calculated based on the weight of Co_3O_4 (73 wt.% cobalt content, determined by EDS, Figure 3-4), because no significant contribution of C itself to the overall capacity is expected. The capacity of Co_3O_4/C_300s was maintained at high levels up to 100 cycles (956 mAh g^{-1}). Although the reversible capacity of the Co_3O_4_300s electrode is higher than that of Co_3O_4/C_300s up to the 60th cycles (978 mAh g^{-1}), a drastic capacity loss is observed after 60 cycles due to the severe increase in electrical resistance and isolation as the result of the formation of a gel-like polymer layer within the hierarchical structure [27,47]. The Co_3O_4 thin film without a carbon matrix shows only a poor capacity of 330 mAh g^{-1} at the 100th cycle. Figure 3-8 displays SEM images of Co_3O_4 and the Co_3O_4/C electrode after 100 cycles. In the case of Co_3O_4, the hierarchical structure completely disappeared due to the volume expansion and aggregation resulting from the conversion reaction and the formation of a polymeric film (Figure 3-8(a)). In contrast, the Co_3O_4/C electrode maintained its shape with only a slight deformation by the polymer layer (Figure 3-8(b) and (c)). Based

on the above results, it can be concluded that this unique structure embedded in a carbonaceous matrix can retain its structural integrity, which is a key factor for ensuring the cycleability of our materials. It is apparent that the amorphous carbonaceous matrix not only provides an elastic buffer space to effectively accommodate the volume expansion that occurs during the cycling process but also prevents aggregation and the electrical isolation of Co_3O_4.

To investigate the role of the preferentially oriented structure and the carbon matrix as a provider for an electrical conductive network, impedance spectra were obtained for the pure Co_3O_4 and Co_3O_4/C electrodes at the 2nd and 100th cycles (Figure 3-9). The Nyquist plots of both electrodes consisted of a semicircle at high frequency, which is correlated with charge transfer resistance on the electrode interface. The semicircle for the pure Co_3O_4 film had much larger diameter compared with that of the Co_3O_4/C thin film at the 2nd cycle. Thereafter, the impedance test of Co_3O_4 at the end of 100 cycles showed an extremely high charge transfer resistance (Figure 3-9(a)). Due to the electrochemical conversion reaction, the interconnective nanoflaky structured Co_3O_4 materials undergo a large volume change, leading to mechanical stress and subsequent structural failure that induce an electrical isolation and contact loss within the as-synthesized electrode, followed by an increase in charge transfer resistance [54,55]. In contrast, it can be clearly seen that the semicircle corresponding to the Co_3O_4/C thin films decreased, as shown in Figure 3-9(b). This behavior indicates that the Co_3O_4 embedded in the carbonaceous matrix are favorable for the formation of a stable SEI film [54,55]. The composite structure appeared to reach a stabilized state, which

support the observed reversible capacity of Co_3O_4/C electrode until 50 cycles (Figure 3-7(d)). After 100 cycles, the elemental distribution of cobalt and carbon in the Co_3O_4/C film was also examined by EDS (Figure 3-10), and Co_3O_4 was confirmed to be uniformly distributed in the carbon matrix even after 100th cycle. From the above results, we conclude that the carbonaceous matrix serves as a conductive path way and induces the formation of a high quality, stable SEI layer. Moreover, the preferentially oriented crystalline structure enables electrons to easily travel to the substrate/electrolyte through a uniformly oriented crystal phase, thereby contributing to the enhanced electrical conductivity and cycleability of the product.

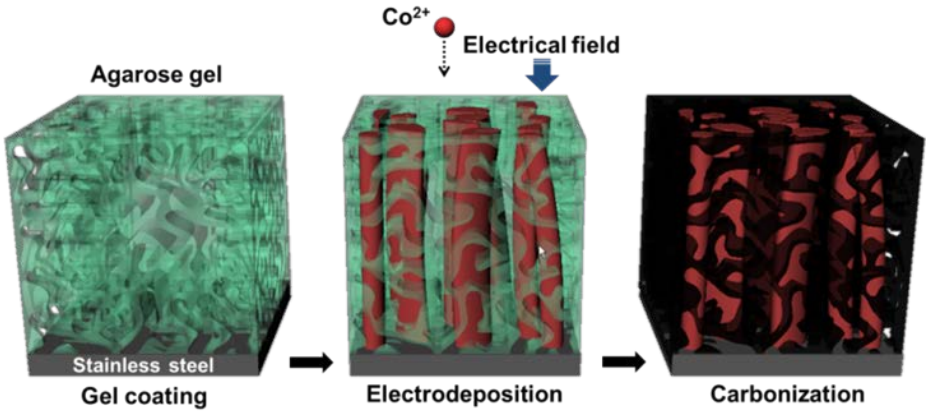

Figure 3-1. Schematic representation of the fabrication process used for preferentially grown Co_3O_4 embedded in a carbon matirix.

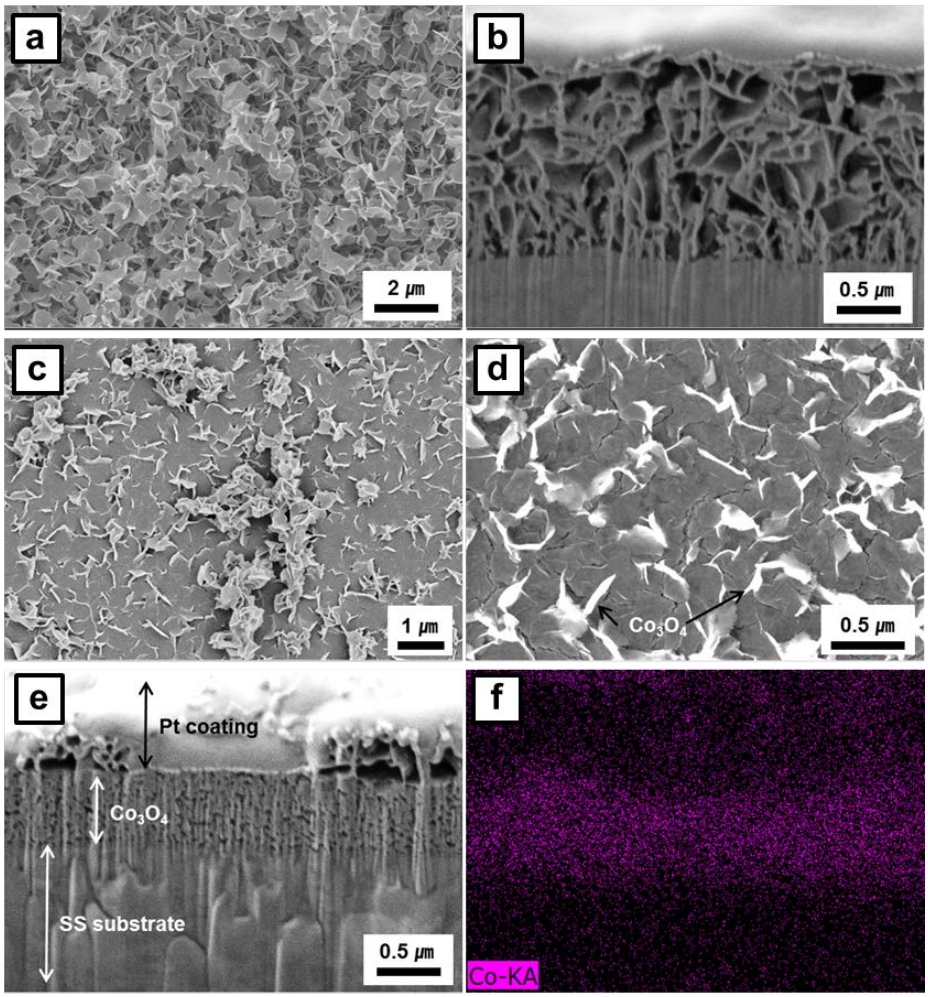

Figure 3-2. SEM images of electrodeposited thin films; (a and b) top and side views of Co_3O_4 electrodeposited for 300s (Co_3O_4_300s) and (c and d) top views of Co_3O_4/C electrodeposited for 300s (Co_3O_4/C_300s). EDS atomic analysis results of side views of Co_3O_4/C_300s film; (e) SEM image and (f) cobalt.

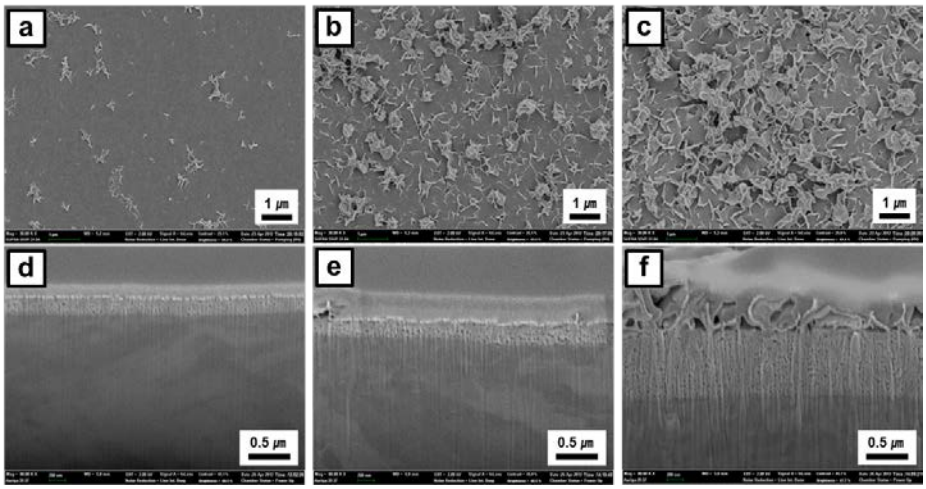

Figure 3-3. SEM images of top and side views of as-synthesized Co_3O_4/C as a function of electrodeposition time; (a and d) 100 s, (b and e) 200 s, and (c and f) 400 s.

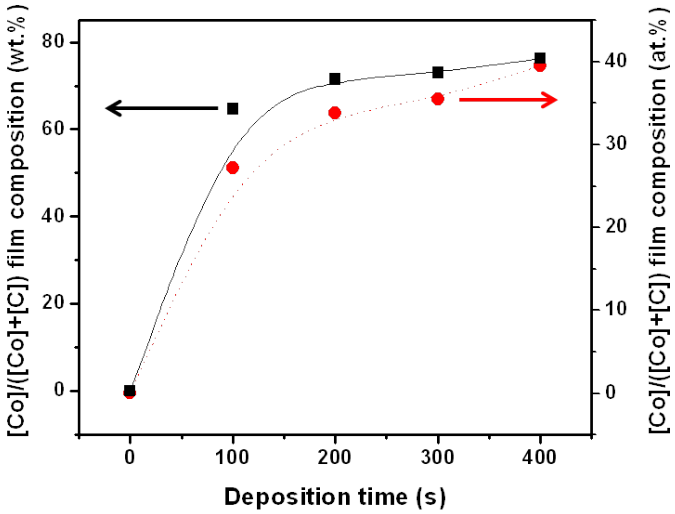

Figure 3-4. Variations in Co content in the Co_3O_4/C composite as a function of electrodeposition time. Each value represents the average of three different deposits. The deviation of the film composition was less than 5 %.

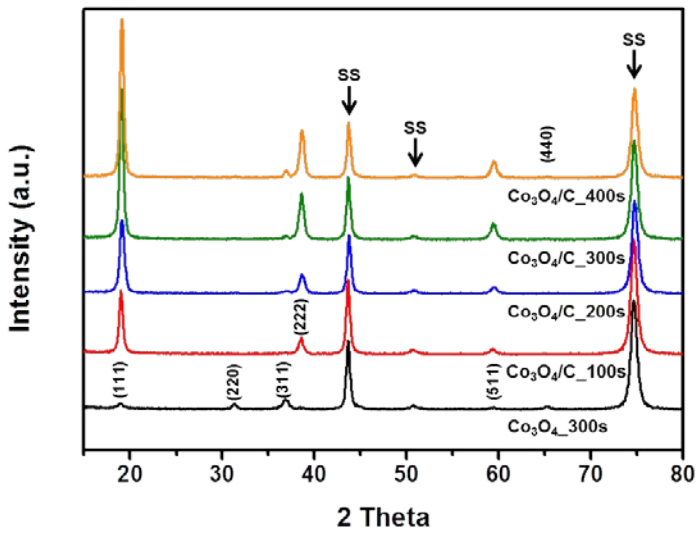

Figure 3-5. XRD patterns of Co_3O_4 and Co_3O_4/C thin films electrodeposited for 100 s (Co_3O_4/C_100s), 200 s (Co_3O_4/C_200s), 300 s (Co_3O_4/C_300s), and 400 s (Co_3O_4/C_400s).

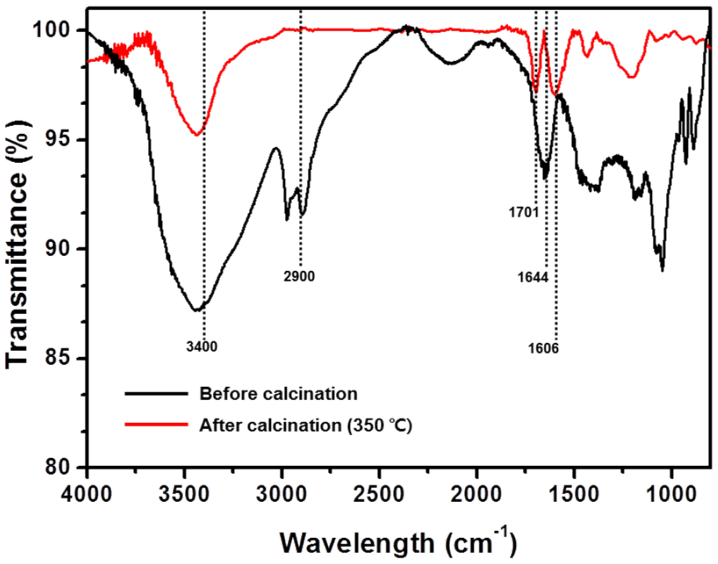

Figure 3-6. IR spectra of agarose gel before and after calcination at 350 ^{o}C.

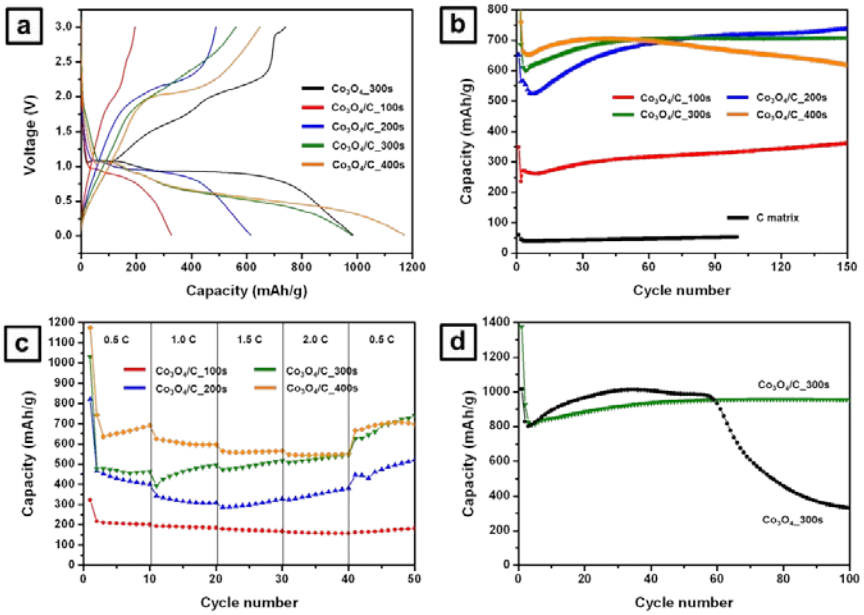

Figure 3-7. Electrochemical performance test of synthesized films; (a) charge–discharge curves of Co_3O_4/C as a function of electrodeposition time at a current density of 890 mA g^{-1} (1 C), (b) cycling performances of C and Co_3O_4/C thin films at 1 C, (c) rate capability of as-synthesized Co_3O_4/C films at various current densities between 445 and 1780 mA g^{-1}, and (d) comparison of the cycling performance of the Co_3O_4_300s and Co_3O_4/C_300s composite at 1 C.

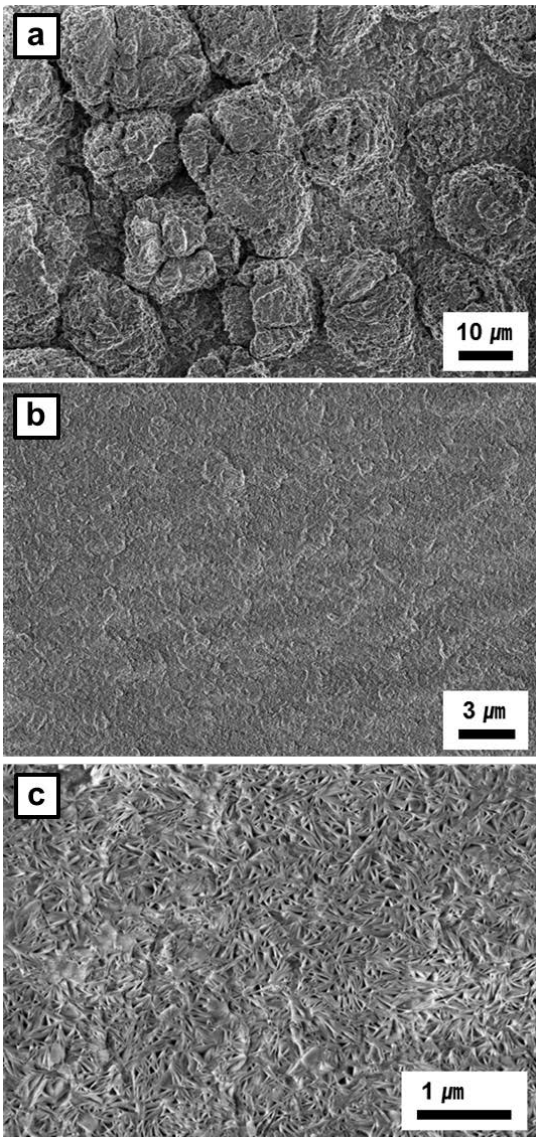

Figure 3-8. SEM images of electrodes after 100 cycles; (a) Co_3O_4_300s and (b and c) Co_3O_4/C_300s.

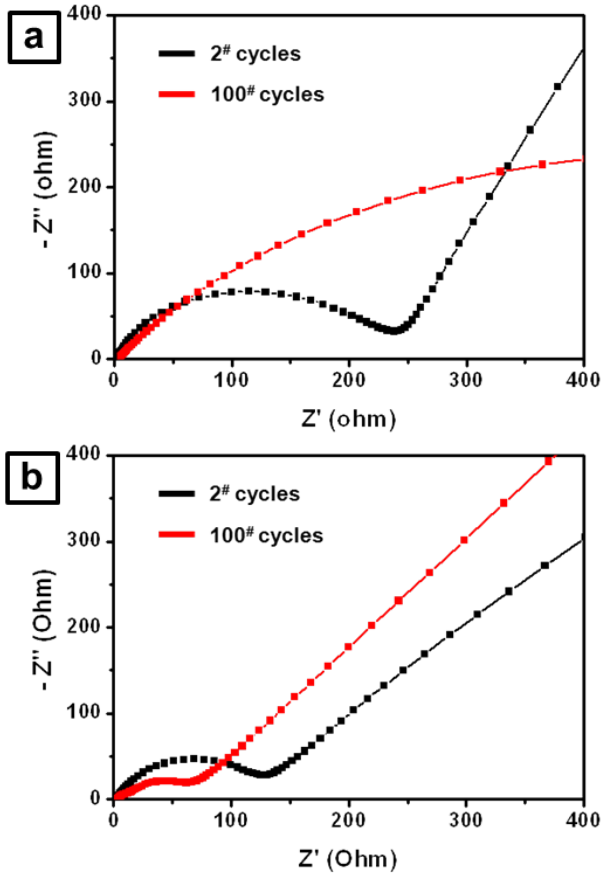

Figure 3-9. Impedance spectra of as-synthesized films: (a) Co_3O_4_300s and (b) Co_3O_4/C_300s.

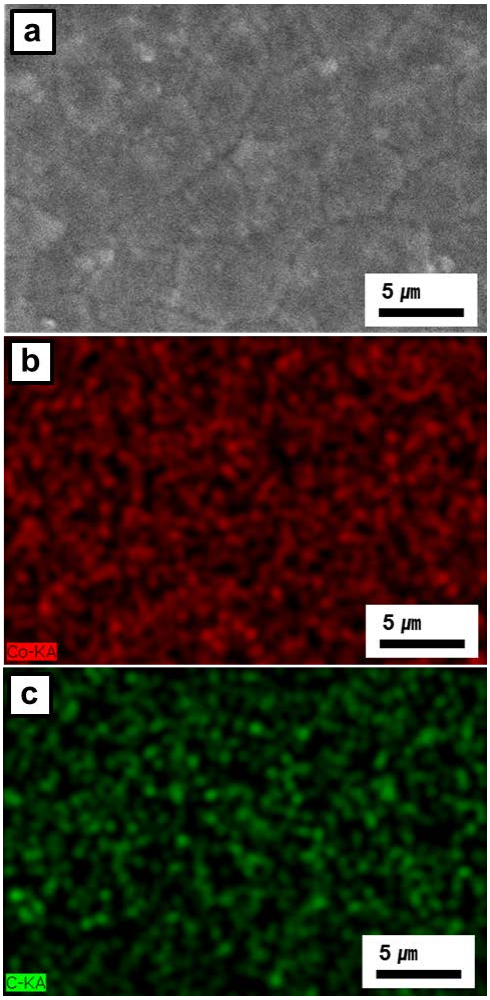

Figure 3-10. EDS atomic analysis results of Co_3O_4/C_300s composite film after 100 cycles; (a) SEM image of thin films, (b) cobalt, and (c) carbon.

3.2 Synthesis of porous NiO materials with preferentially oriented crystalline structure with enhanced stability as Li-ion battery anodes

3.2.1 Introduction

Due to their high energy density and power density, lithium-ion batteries (LIBs) are one of the most promising candidates for use in energy storage and conversion devices. In particular, recent progress in the study of alternative anode materials for LIBs has stimulated rapid development in this field. Electrochemically active metal oxides, such as Co_3O_4 [24,63,65], NiO [78-80], Fe_2O_3 [81], and MnO_2 [82], and carbon-based composites thereof [83-85] have been exploited as the anode materials for LIBs. Although a variety of techniques including an in-situ reduction process [86], a sol-gel process [87], and chemical vapor deposition [88] have been widely used in the fabrication of the above-mentioned materials, electrodeposition is a particularly attractive technique, in that the coating mass, thickness, and morphology of the metal oxide thin film can be easily controlled by adjusting the applied current and bath composition [38,40]. In addition, the electrode can be directly synthesized onto a substrate without any complicated processing step involving the addition of a binder or an electrical conductor. Due to the different shrinkage or expansion properties between the deposited thin film and the substrate, however, peeling or cracking of the active material layers occur on the substrate, which are typically the result of the heat treatment used in the crystallization process, which can result in poor reversible capacity and

electronic conductivity [89,90].

To achieve an enhanced structural electrochemical stability, numerous efforts have been devoted to the development of new types of templating techniques [91,92]. Biopolymer templates including cellulose [93], dextran-based polymers [94], and agarose [61] have been used in a variety of applications due to their ease of preparation, low cost, and environmental benignness, and the fact that they are freely soluble in water. Among the above-mentioned materials, agarose gels, with sub-micrometer porous network structures, have numerous applications for biological research [56] as well as serving as a promising organic template for the synthesis of porous metal oxides using the sol-gel method [15,56]. An agarose polymer matrix not only has an excellent film-forming ability on the substrate and is highly stable in an aqueous solution but also can effectively deliver metallic precursors to the interior of the gel [61], which could be used as a meditative template for the fabrication of highly mechanically stable metal oxide thin films by electrodeposition [61]. In addition, the electrodeposited metal hydroxide/agarose gel thin film can be readily converted into a well-dispersed metal oxide embedded on a carbonaceous matrix by heat treatment under nitrogen atmosphere [62]. The carbonaceous matrix effectively alleviates the volume expansion and aggregation of nanoparticles. Moreover, the carbonaceous layer can function as a highly conductive matrix, thus enabling good electrical contact with the metal oxide and can serve as a preventive measure against electrode pulverization. More importantly, during the electrodeposition process, the direction of diffusion of metallic precursors can

be regulated by the applied electric field through the hydrogel, resulting in the isotropic crystal growth of the metal oxide [63]. The one-dimensional structure enables electrons to easily travel to the electrode/electrolyte interface.

Among the transition metal oxides, NiO is one of the promising anode materials for use in LIBs because of its high theoretical capacity (718 mAh g^{-1}) [95], which would be expected to meet the increasing demand for high performance LIBs. Practical applications, however, continue to be restrained by detrimental effects related to its structural and electrochemical properties, resulting from the pulverization of active materials by the large volume change that occurs during the cycling process. In this study, we demonstrate the use of agarose-mediated electrodeposition method as a simple strategy for the synthesis of preferentially grown nickel oxide embedded in a conducting carbonaceous matrix (NiO/C) as an advanced anode material for use in LIBs. The electrodeposited composites can efficiently utilize the combined merits of NiO with a preferred orientation and a carbonaceous matrix, resulting in superior electrochemical properties with a large reversible capacity, excellent cycling stability, and an enhanced conductivity as an anode material in LIBs. As a result, agarose gel-templated electrodeposition represents a promising procedure for the synthesis of inorganic-organic hybrid materials for energy storage applications.

3.2.2 Experimental

3.2.2.1 Preparation of preferentially grown NiO embedded in a carbonaceous matrix

The NiO/C was prepared as follows. A 1% (w/v) solution of agarose powder was prepared in deionized (DI) water with vigorous stirring. The solution was heated to boiling using a microwave oven. For the preparation of agarose gel template, the above aqueous solution was then cast on stainless steel (SS) substrates (2 x 4 cm^2) by a dip-coating method, followed by a 4-hour period of gelation at room temperature. The plating bath was comprised of 0.05 M of $Ni(NO_3)_2$ and 0.075 M of $NaNO_3$ in DI water. The electrodeposition was performed potentiostatically at – 1.0 V (vs Ag/AgCl) for 300 s) at room temperature. The agarose coated SS was employed as a working electrode. A Pt plate and Ag/AgCl were used as the counter electrode and reference electrode, respectively. After electrodeposition, the as synthesized films were rinsed with DI water and dried at room temperature for 24 h, followed a heat treatment at 350 ^oC for 2 h under a nitrogen atmosphere. For comparison, a pure NiO film without an agarose template was electrodeposited following the similar procedure without an agarose template for 300 s.

3.2.2.2 Materials characterization

The NiO/C composite material was characterized by scanning electron microscopy (SEM, Carl Zeiss, SUPRA 55VP), focused-ion beam microscopy (FIB, Carl Zeiss, AURIGA), energy dispersive spectrometry (EDS, Bruker, Xflash5030 detector), X-ray diffraction (XRD, Rigaku, D/max-2200), and fourier transform-infrared spectroscopy (FT-IR, Thermo Scientific, Nicolet 6700).

3.2.2.3 Electrochemical measurement

Electrochemical experiments were performed using a conventional coin cell (CR2032). The electrolyte solution was a 1 M $LiPF_6$ solution in ethyl carbonate and diethyl carbonate (1:1 by volume). The cells were assembled in an argon-filled glove box using as-prepared films as the working electrode. A lithium foil and microporous polypropylene were used as the counter electrode and separator, respectively. The galvanostatic discharge/charge measurements were conducted on a battery tester (WonA tech, WBCS3000) between 0.01 and 3.0 V with a constant current density of 718 mA g^{-1} (1 C). The electrochemical impedance spectroscopy (EIS) of the electrode was performed on an electrochemical workstation (WonA tech, ZIVE SP2). The frequency of EIS ranged from 0.01 Hz to 200 kHz at the open circuit potential.

3.2.3 Results and discussion

The SEM images and EDS atomic analysis data for the electrodeposited thin films after a heat treatment 350 ^{o}C for 2 h are shown in Figure 3-11. Although the as-synthesized NiO film without an agarose gel template has a homogeneous dense and flat structure which is constructed by the aggregation of numerous small nanoscale-sized particles (Figure 3-11(a) and (b)), a number of severe cracks are clearly observed. The cracked nature of the film is typically attributed to contraction and dehydration of hydroxide precursors by drying, during the heating process [89,96]. In contrast, in the case of an agarose gel template, the deposited film layer is relatively smooth and devoid of cracks (Figure 3-11(c) and (d)). The electrodeposited NiO is homogeneously embedded in the carbonaceous matrix. Only minor amounts of NiO nanoparticles are observed on the surface as deposited film thickness increases to more than the thickness of the agarose gel template. From the above results, the carbonaceous matrix appears to efficiently act as a buffer region, preventing the cracking of deposits. To further confirm the elemental distribution of nickel and carbon in the deposits, EDS mapping was employed, and the results are shown in Figure 3-11(e) and (f). Both nickel and carbon are very uniformly distributed on the electrode surface. The average atomic ratio of Ni to C is about 61.3:38.7 at.%, respectively. This result demonstrates that a NiO/C composite with a high uniformity can be successfully prepared by electrodeposition using agarose gel template.

Cross-section SEM images of electrodeposited films after the heat

treatment are shown in Figure 3-12. The NiO films without template have a homogeneous densely-packed structure containing aggregates comprised of small nanoparticles and there are fewer voids in the deposited layer. Furthermore, the deposited NiO loses its structural rigidity, and consequently separates from the current collector. In contrast, NiO/C films not only have a smooth surface and uniform thickness but also adhere well to the substrate. More importantly, the interconnected porous structure is well-developed in the deposited layer, which facilitates the penetration of the electrolyte, thus permitting Li^+ ions to react more easily with more active sites. Moreover, this structure is beneficial for alleviating the large volume change that occurs during the cycling process. This result provides a clear demonstration to show that an agarose gel template plays an essential role in the formation of a porous NiO film with enhanced structural stability.

Figure 3-13(a) displays XRD patterns for NiO and NiO/C films that were electrodeposited on a stainless steel substrate after calcination. These patterns clearly indicate the influence of the agarose gel template on the structural properties of the product. For the NiO film, the major diffraction lines correspond to (111), (200), and (220) crystalline of cubic NiO phase (JCPDS 47-1049). In the case of the NiO/C film, however, an unusually strong (111) and weak (222) diffraction peaks are observed. This result can be attributed to anisotropic ion diffusion inside the agarose gel [63]. The gel template is able to provide pathways for the precursor ions under an applied electric field, and Ni^{2+} ions linearly and compulsorily migrate inside the gels. Consequently, the ions are orientated in one direction, followed by a reduction process on the

surface of the substrate. This is entirely different from findings of previous reports on the electrodeposition of NiO that were simply grown on bare substrates [40]. The small intensity of the (220) reflection can be attributed to the outward growth of NiO nanoparticulates from the agarose gel template. It should also be noted that the agarose gel template has a significant effect on the crystalline phase of the electrodeposited NiO. FT-IR measurements were carried out to gain insights into the chemical transformation that occurs when the agarose gel is converted into carbonaceous products through a heat treatment under a nitrogen atmosphere. IR spectra of the agarose gel before and after calcination are shown in Figure 3-13(b). Prior to the heat treatment, the characteristic peaks can be assigned to an –OH stretching vibration (around 3400 cm^{-1}). This band is correlated to the OH banding mode (1645 cm^{-1}), which arises from the hydroxyl groups of agarose and adsorbed water molecules. The bands around 2900 cm^{-1} are –CH stretching vibrations from the agarose gel. In the NiO/C composite, the characteristic peaks at 1700 and 1605 cm^{-1} are assigned to C=O and C=C vibrations corresponding to the carbonaceous matrix, respectively. Furthermore, the peaks at 1000-1450 cm^{-1} and the broad band at 3000-3750 cm^{-1} decrease significantly, indicating that dehydration occurred during the carbonization process [75-78]. This can be attributed to the fact that as synthesized $Ni(OH)_2$/agarose gel film is readily converted into a NiO/C composite by the carbonization process under a nitrogen environment at 350 ^oC for 2h.

Figure 3-14(a) and (b) show a comparison of the galvanostatic charge-discharge behavior of bare NiO and NiO/C thin films at a constant current of

718 mA g^{-1} (1 C). The specific capacities were calculated based on the total mass of the active materials including the carbonaceous matrix. The first discharge and charge capacities are found to be 997 and 584 mAh g^{-1} for the pure NiO, corresponding to an initial columbic efficiency of 58.6% (Figure 3-14(a)). By contrast, the NiO/C composite shows a large discharge capacity of 1140 mAh g^{-1} and a reversible capacity of 767 mAh g^{-1}, corresponding to an improved initial columbic efficiency of 67.3% (Figure 3-14(b)). In addition, two potential regions can be observed in the discharge profile. Although a long voltage plateau is found around 0.6 V for both samples, which is the result of the reduction of NiO to Ni and the formation of a solid electrolyte interface (SEI) film, the potential region around 0.75 V corresponding to the formation of SEI and the Li-storage in carbonaceous matrix is not visible for the NiO film [77]. The introduction of a carbonaceous matrix indicates the existence of a synergetic effect that plays a role in the enhanced reversible capacity. The initial capacity loss could be attributed to the incomplete conversion reaction and irreversible lithium loss due to the formation of SEI [95]. The high reversibility and enhanced stability of the NiO/C composite film is even more strongly highlighted, as shown in Figure 3-14(c). The cyclic performance was evaluated at a current density of 1 C between 0.01 and 3.0 V. The reversible capacity of the pure NiO electrode rapidly drops to 203 mAh g^{-1} after 100 cycles, only a 35% retention of the initial charge capacity. In contrast, the NiO/C composite film exhibits a high reversible capacity of 604 mAh g^{-1} at a high level for up to 100 cycles, which is almost three times higher than that of the NiO film. The retention of capacity is maintained

above 78%. More importantly, the reversible capacity of NiO/C electrode increases slightly from the 2nd cycles and reaches 864 mAh g^{-1} at the 10th cycle. These results can be attributed to gradual activation by the formation of a stable SEI within the interconnected porous structure of the NiO during the first several cycles [95,97]. The structure appears to reach a stabilized state, which is consistent with the observed extra capacity until 10 cycles. The rate capability of NiO/C was also demonstrated at various rates from 0.5 to 2 C, as shown in Figure 3-14(d). The sustained nature of the composite film is clearer at a high current density. Upon increasing the current density to 1, 1.5, and 2 C, the NiO/C is still able to deliver a discharge capacity of 693, 621, and 563 mAh g^{-1}, respectively. It is obvious that, although a current increase leads to a gradual decrease in reversible capacity, the current density has little impact on the overall process. Based on the above results, the high reversibility and excellent cycling stability can be explained as follows: 1) the interconnected porous NiO structure could be favorable for Li^+ diffusion to more active sites. 2) the sufficient void volume of the structure helps to accommodate the volume expansion. 3) the carbonaceous matrix prevents aggregation and the electrical isolation of active materials, and preserves the integrity of the overall electrode from disconnecting the current collector as an elastic buffer space.

In order to gain further insights into the role of the carbonaceous matrix and the preferential orientated structure as a provider for an electrical conductive network, EIS measurements of the NiO and NiO/C electrodes were conducted after the 10th and 100th cycles, as shown in Figure 3-15. Nyquist plots

indicate that the diameter of the semicircle for NiO/C film in the medium frequency region is much smaller than that of NiO, indicating that NiO/C composite electrode possesses lower charge transfer resistances at the 10th cycle [51]. After cycling, the impedance data at the end of 100 cycles shows that the diameter of the semicircle in the medium frequency region for NiO is much larger than that for the electrode before cycling, indicating increased charge transfer resistances (Figure 4-15(a)). During continued cycling, it is possible that the NiO materials could undergo a large volume change by the electrochemical conversion reactions, leading to mechanical stress and subsequent pulverization of the active layers, followed by electrical isolation and contact loss within the as-synthesized electrode. In contrast, it can be clearly seen that the semicircle for the NiO/C composite is smaller than that for the electrode before cycling (Figure 3-15(b)). This behavior indicates that NiO embedded in a carbonaceous matrix is favorable for the formation of a stable SEI film. In addition, the intercept at the real axis at a high frequency, corresponding to the ohmic resistance, is nearly constant after cycling, which suggests good contact between the current collector and the electrode, as well as the structure integrity of the NiO/C electrode (Figure 3-15(b)) [98]. To further confirm the structure integrity of the as-synthesized films, the evolution of the morphology and structure of NiO and NiO/C were investigated, as shown in Figure 3-16. The SEM image of the NiO film after 100 cycles clearly shows that the electrode suffers from severe cracking and that the active layers have become pulverized. Subsequently, the deposited NiO deteriorates with most of the film being peeled off from the substrate. In

contrast, the NiO with a carbonaceous matrix do not suffer from observable morphological changes and retains its structural integrity with only a slight deformation. On the basis of the above results, the improved electrochemical performance of the NiO/C composite could be reasonably attributed to the advantageous combination of preferentially grown NiO and a carbonaceous matrix. The matrix induces the formation of stable SEI layers and improves the conductivity of the composite. The flexibility of the matrix can maintain structural integrity by suppressing the pulverization of active materials and by accommodating volume expansion that occurs during the cycle process. Moreover, the preferentially oriented crystalline material can assist electron transport between the substrate and electrolyte, thereby contributing to the enhanced electrical conductivity and cycleability of the product.

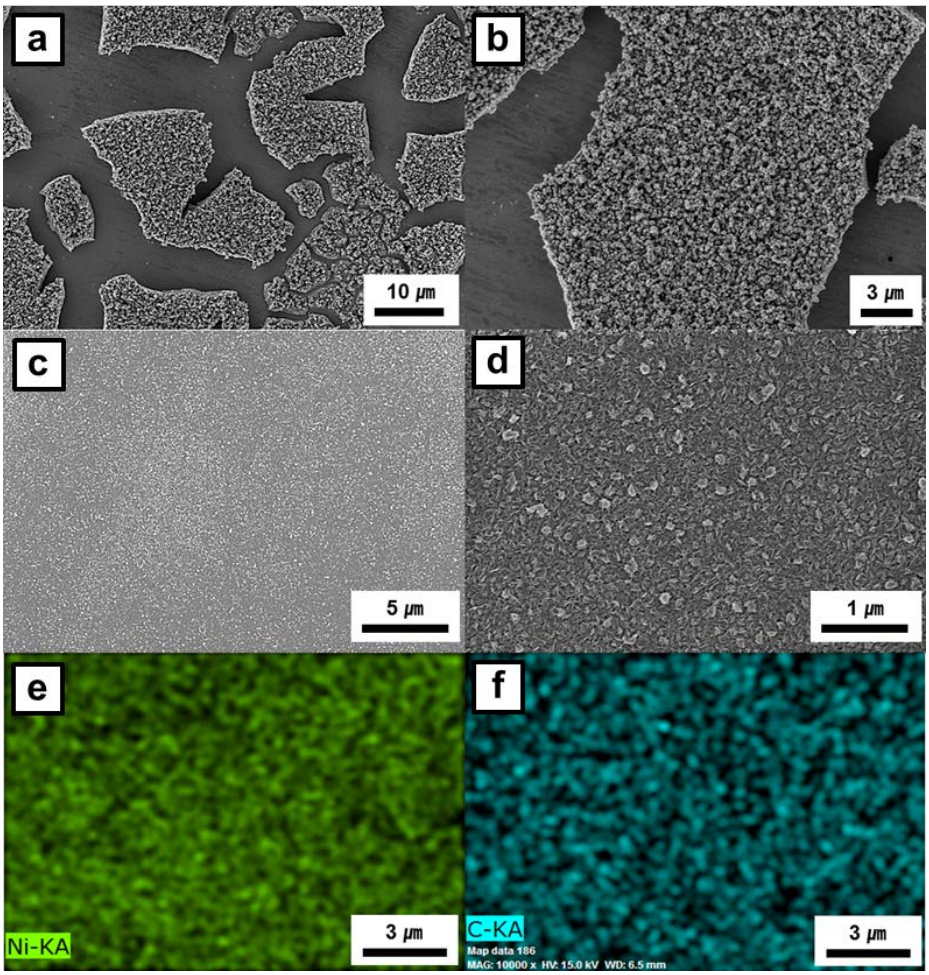

Figure 3-11. SEM images of electrodeposited thin films; (a and b) NiO, (c and d) NiO/C after calcination at 350 _C for 2 h under a nitrogen atmosphere. EDS atomic analysis results for NiO/C films; (e) nickel and (f) carbon.

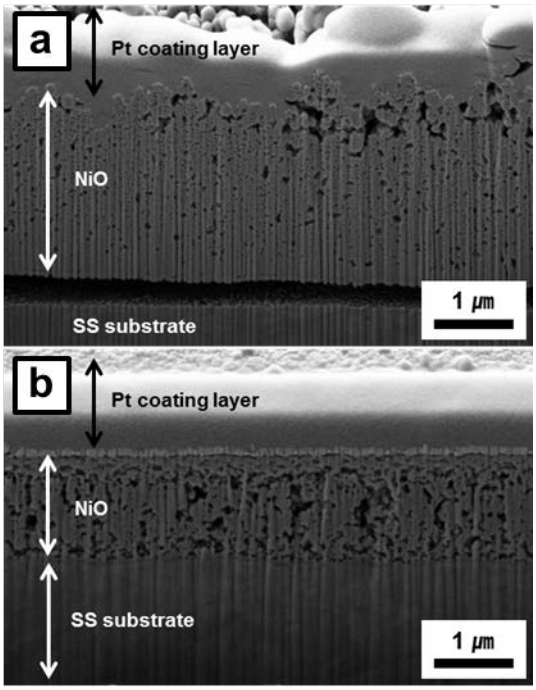

Figure 3-12. Side views of SEM images of electrodeposited thin films; (a) pure NiO and (b) NiO/C films.

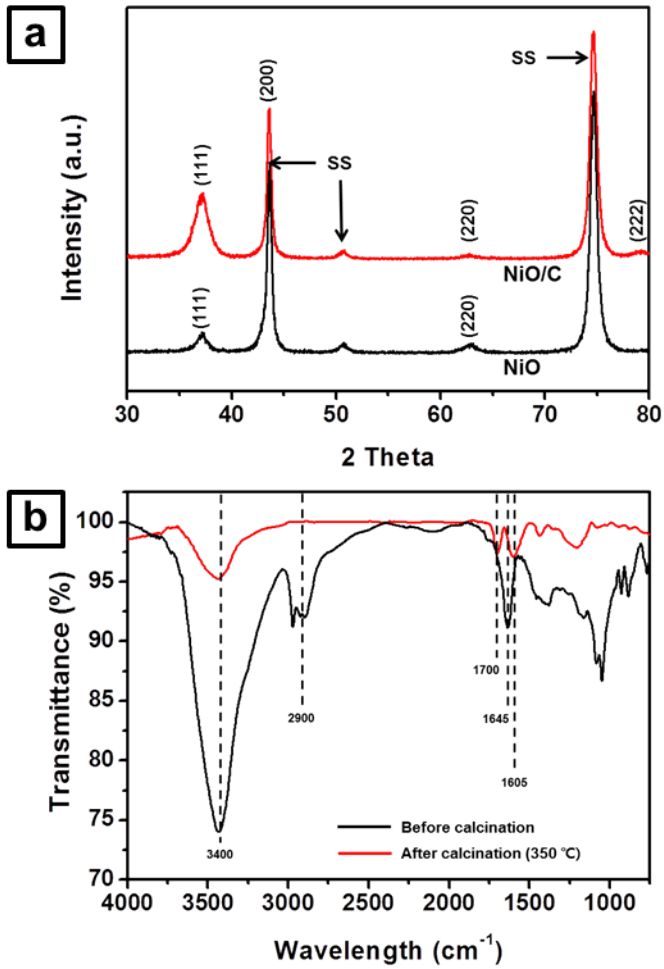

Figure 3-13. (a) XRD spectra of NiO and NiO/C thin films after calcination and (b) IR spectra of an agarose gel before and after calcination at 350 _C for 2 h under a nitrogen atmosphere.

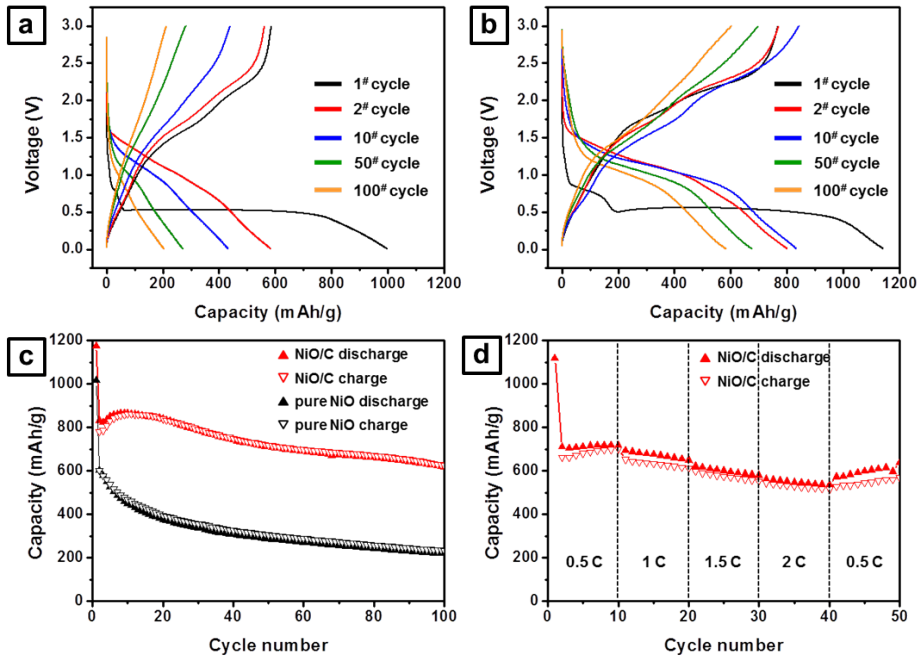

Figure 3-14. Electrochemical performance test of electrodeposited films; charge/discharge curves of (a) NiO film and (b) NiO/C film, (c) cycleability of NiO and NiO/C films with a current density of 718 mA g^{-1} (1 C), and (d) rate capability test of the NiO/C film.

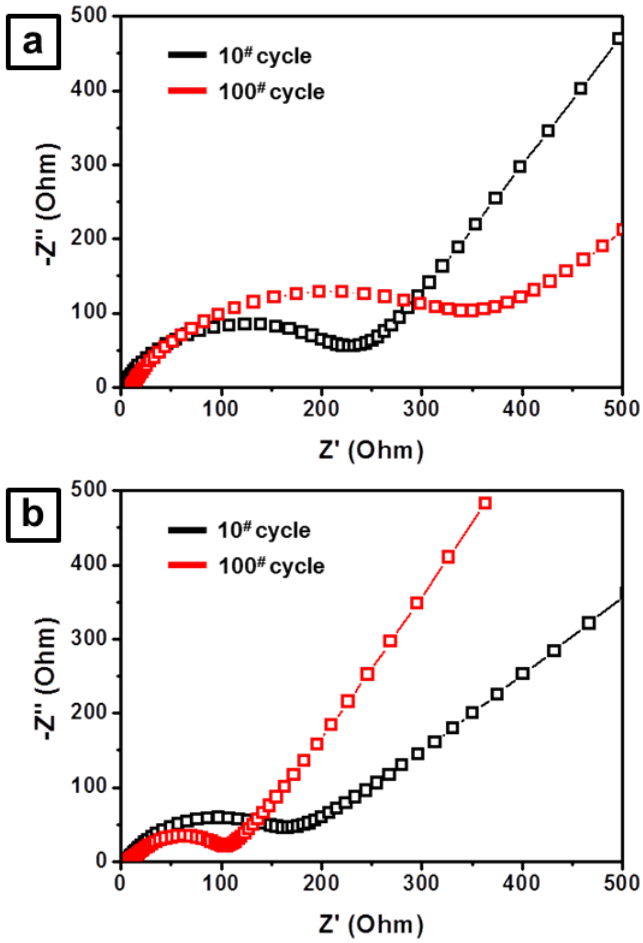

Figure 3-15. Impedance comparison curves; (a) NiO and (b) NiO/C.

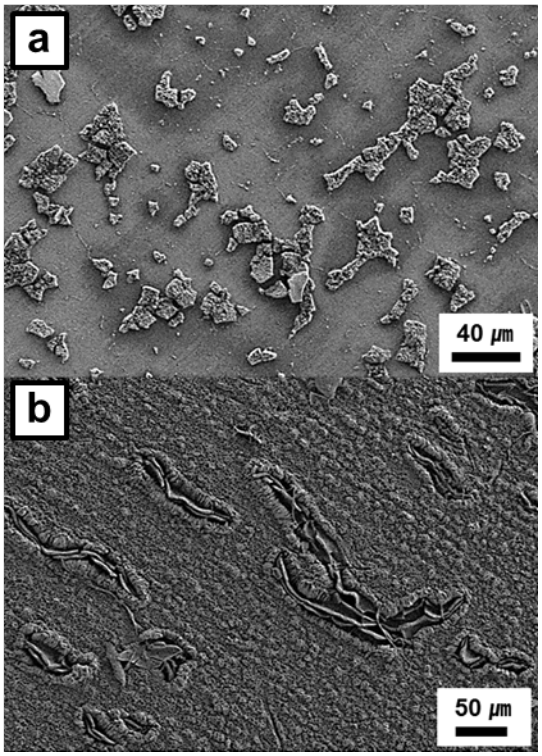

Figure 3-16. SEM images of electrodes after 100 cycles; (a) NiO and (b) NiO/C.

Chapter 4. Summary and Conclusions

Base on the finding that the PEI modified graphene oxide can be co-electrodeposited with positively charged metal precursors under cathodic conditions, the one-step synthesis of graphene/metal oxide electrode materials is successfully demonstrated via the PEI-mediated strategy. Graphene oxides were chemically modified by treatment with PEI. Firstly, the resulting PEI-modified graphene oxides were then coelectrodeposited with a cobalt precursor under cathodic conditions. The PEI-modified graphene oxides were well dispersed across a large surface area. The as-synthesized graphene/Co_3O_4 exhibited an enhanced reversible capacity, cycling performance, and electronic conductivity as an anode material for LIBs. These improvements can be explained by an excellent ion diffusion and conductivity of the graphene/Co_3O_4 thin films. Secondly, the interconnected NiO nanoparticles that are uniformly electrodeposited onto a graphene surface are successfully prepared. The resultant thin film can be directly used for a LIB anode material. The reversible capacity and electronic conductivity of the graphene/NiO are significantly improved. These enhancements result from the synergistic effect of the graphene, which can assist electron transport and participate in the lithium storage process. We conclude that co-electrodeposition, when used in conjunction with PEI-GO, can result in enhanced electrochemical properties of the transition metal oxide for LIB anodes.

The agarose polymer matrix can be used as a meditative template for the

fabrication of metal-based thin films by electrodeposition because the thin polymer layer not only can linearly and compulsorily deliver metallic precursors inside the gel but also can be converted into a carbonaceous matrix by a carbonization. We demonstrated an agarose-mediated electrodeposition that allows the direct growth of vertically aligned and close-packed and porous Co_3O_4 embedded in a carbonaceous matrix. These structures were composed of preferentially oriented (111) crystalline substances. The resultant deposits embedded in the carbonaceous matrix can be directly used for lithium ion battery anodes without adding any additional ancillary materials. The as-synthesized Co_3O_4/C exhibited an enhanced cycle performance, lithium storage capacity, and electronic conductivity. This superior cyclic stability resulted from the synergetic effect of the carbonaceous matrix, which accommodates the volume expansion and retards the development of a thick SEI that can lead to electrical isolation. In addition, we expect that the preferential oriented structure of Co_3O_4 can assist electron transport. In addition, porous NiO/C composite films were also successfully prepared by agarose-gel templated electrodeposition. The structures are composed of preferentially orientated (111) crystalline substances. The resulting composite films can be directly used for an LIB anode material. The as-synthesized NiO/C exhibits a significantly improved cycle stability, reversible capacity, and electrical conductivity, compared with bare NiO films, which is primarily attributed to the synergistic effect of the conductive carbonaceous matrix and the preferentially grown NiO with an interconnected porous structure. The present synthetic protocol opens up new opportunities for the synthesis of

other materials with promising applications in supercapacitors and photocatalysts.

In conclusion, the electrochemical reactions of lithium with active materials synthesized by polymer-mediated strategy have been investigated. The variation of discharge capacity with cycle number is shown in Figure 4-1. The nanostructured electrode materials exhibited excellent capacities that exceed the theoretical values for the first 10-20 cycles, which are conversion reactions. This behavior has been attributed to the increasing formation of a polymeric surface layer on these high surface areas of as-synthesized materials. The capacities of graphene/Co_3O_4, graphene/NiO, and NiO/C began to be decreased with the increase of the cycle numbers. In the cases of graphene/Co_3O_4 and graphene/NiO, the decreases of capacities were examined to be severe. This could be due to the effects of pulverization and deterioration of the active materials, which are caused by the large specific volume change during the cycling. Moreover, it was clearly proved that the existence of the graphene contributed on the increase of the total capacities, not the cyclic stability. In contrast, the high reversible capacity of Co_3O_4/C was retained without any fluctuation of capacity at large number of the cycle, 100 cycles. Based on the above results, I concluded that agarose gel-mediated electrodeposition is a promising method for having the both of high electrochemical property and stability.

These results show that the electrodeposition, when used in conjunction with polymer mediation, can be extended to the synthesis of other materials for use in various applications.

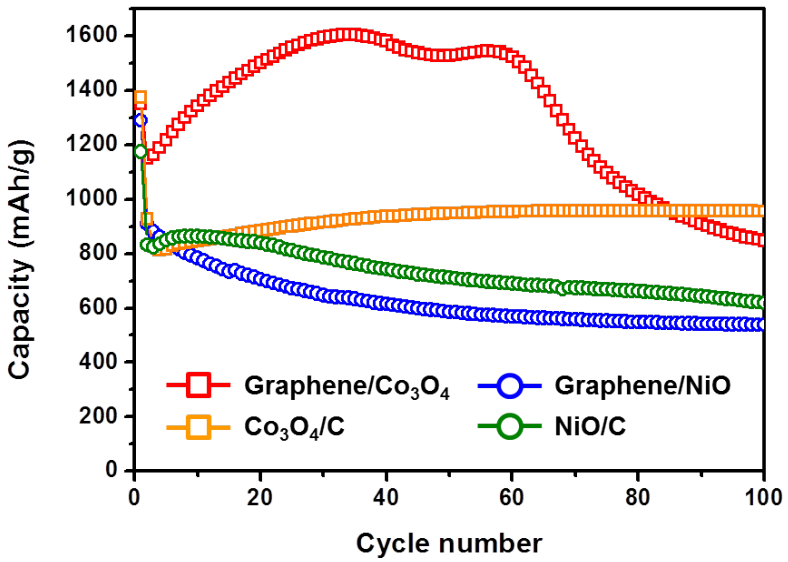

Figure 4-1. Discharge capacities as a fuction of cyclenumbers for graphene/Co_3O_4, graphene/NiO, Co_3O_4/C, and NiO/C composites.

Chapter 5. Recommendations for Further Research

The recommendations for further research are summarized as follows;

1) For the development of high-performance energy storage system, organic materials are playing increasingly important roles. The currently reported energy storage media are basically inorganic materials such as metal and transition metal oxides. It is necessary to develop renewable organic energy storage materials from the viewpoint of sustainability and ecoefficiency. Organic/inorganic hybrid electrode materials have been continuously reported to show desirable electrochemical properties, and it is predicted that biomass could be used as electrodes for lithium-ion battery and electrocatalysis in the future.
2) The significant progress has been made in nanostructured electrode materials. However, there are still major challenges for achieving commercially viable electrode materials because the nanostructured materials may be more difficult to synthesize and organic/inorganic hybridization may be difficult to control. New simple and controllable synthesizing method is essentially required for their practical usage. Once these problems have been solved, it would be become possible to prepare low-cost, active and robust electrode materials for the ultimate commercialization.

3) The combination of theoretical calculations and experimental investigations will promote the exploration of high-performance electrode materials. Computational simulation and modeling are an effective way to predict the properties and optimize the composition of electrode materials and catalysts used in energy storage systems. Therefore, further study will be required to significantaly improve the efficiency of developing novel energy storage materials through the theoretical prediction.

Bibliography

[1] C. Liu, F. Li, L. –P. Ma, H. –M. Cheng, *Adv. Energy Mater.* **22** (2010) E28.

[2] P. G. Bruce, B. Scorosati, J. –M. Tarascon, *Angew. Chem. Int. Ed*. **47** (2008) 2930.

[3] M. Gyu, J. Cho, *Adv. Funct. Mater*. **19** (2009) 1497.

[4] S. Park, Y. Shao, J. Liu, Y. Wang, *Energy Environ. Sci*. **5** (2012) 9331.

[5] B. Scrosati, J. Garche, *J. Power Sources* **195** (2010) 2419.

[6] S. Zhang, Y. Shao, G. Yin, Y. Lin, *J. Mater. Chem. A* **1** (2013) 4631.

[7] B. Gao, P. Jiang, H. Lei, *Mater. Lett*. **60** (2006) 3398.

[8] B. Gao, F. An, K. Liu, *Appl. Surf. Sci*. **253** (2006) 1946.

[9] Y. Pang, G. Zeng, L. Tang, Y. Zhang, Y. Liu, X. Lei, Z. Li, J. Zhang, G. Xie, *Desalination* **281** (2011) 278.

[10] C. Liu, K. Wang, S. Luo, Y. Tang, L. Chen, *Small* **7** (2011) 1203.

[11] J. Li, B. L. Armstrong, J. Kiggans, C. Daniel, D. L. Wood, *J. Electrochem. Soc*. **160** (2013) A201.

[12] X. Wang, C. E. Egan, M. Zhou, K. Prince, D. R. G. Mitchell, R. A. Caruso, *Chem. Comm*. **29** (2007) 3061.

[13] T. Singh, T. J. Trivedi, A. Kumar, *Green Chem*. **12** (2010) 1029.

[14] H. Firouzabadi, N. Iranpoor, F. Kazemi, M. Gholinejad, *J. Mole. Catal. A* **357** (2012) 154.

[15] J. Zhou, M. Zhou, R. A. Caruso, *Langmuir* **22** (2006) 3332.

[16] K. S. Novoselov, A. K. Geim, S. V. Morozov, D. Jiang, M. I. Katsnelson, I. V. Grigorieva, S. V. Dubonons, A. A. Firsov, *Nature* **438** (2005) 197.

[17] J. R. Dahn, T. Zheng, Y. H. Liu, J. S. Xue, *Science* **270** (1995) 590.

[18] Z. -S. Wu, W. Ren, L. Wen, L. Gao, J. Zhao, Z. Chen, G. Zhou, F. Li, H.-M. Cheng, *ACS Nano* **4** (2010) 3187.

[19] J. -Z. Wang, C. Zhong, S. Lei, H. Chou, K. Liu, *Electrochem. Comm.* **12** (2010) 1467.

[20] L. Chen, Y. Tang, K. Wang, C. Liu, S. Luo, *Electrochem. Comm*. **13** (2011) 133.

[21] S. Park, K. Lee, G. Bozoklu, W. Cai, S. T. Nguyen, R. S. Ruoff, *ACS Nano* **2** (2008) 572.

[22] D. Yu, L. Dai, *J. Phys. Chem. Lett.* **1** (2010) 467.

[23] D. C. Marcano, D. V. Kosynkin, J. M. Berlin, A. Sinitskii, Z. Sun, A. Slesarev, L. B. Alemany, W. Lu, J. M. Tour, *ACS Nano* **4** (2010) 4806.

[24] W. L. Yao, J. Yang, J. L. Wang, Y. Nuli, *J. Electrochem. Soc*. **155** (2008) A903.

[25] L. Tal, J. Zai, K. Wang, H. Zhang, M. Xu, J. Shen, Y. Su, X. Qian, *J. Power Sources* **202** (2012) 230.

[26] P. Poizot, S. Laruelle, S. Grugeon, L. Dupont, J. -M. Tarascon, *Nature* **407** (2000) 496.

[27] K. M. Shaju, F. Jiao, A. Débart, P. G. Bruce, *Phys. Chem. Chem. Phys*. **9** (2007) 1837.

[28] C. Liu, F. Li, L. P. Ma, H. M. Cheng, *Adv. Mater*. **22** (2010) E28.

[29] Y. G. Guo, J. D. Hu, L. J. Wan, *Adv. Mater*. **20** (2008) 2878.

[30] G. X. Wang, B. Wang, X. L. Wang, J. Park, S. X. Dou, H. Ahn, K. Kim, *J. Mater. Chem*. **19** (2009) 8378.

[31] G. Wang, X. Shen, J. Yao, J. Park, *Carbon* **47** (2009) 2049.

[32] E. J. Yoo, J. Kim J, E. Hosono, H. Zhou, T. Kudo, I. Honma, *Nano Lett*. **8** (2008) 2277.

[33] X. –J. Zhu, J. Hu, H. –L. Dai, L. Ding, L. Jing, *Electrochim. Acta* **64** (2012) 23.

[34] G. Zhou, D. –W. Wang, F. Li, L. Zhang, N. Li, Z. –S. Wu, L. Wen, G. Q. Lu, H. –M. Cheng, *Chem. Mater*. **22** (2010) 5306.

[35] Y. Si, E. T. Samulsk, *Chem. Mater*. **20** (2008) 6792.

[36] R. Pascricha, S. Gupta, A. K. Srivastava, *Small* **20** (2009) 2253.

[37] E. J. Yoo, T. Okata, T. Akita, M. Kohyama, J. Nakamura, I. Honma, *Nano Lett*. **9** (2009) 2255.

[38] Y. Tan, S. Srinivasan, K. S. Choi, *J. Am. Chem. Soc*. **127** (2005) 3596.

[39] X. H. Xia, J. P. Tu, J. Y. Xiang, X. H. Huang, X. L. Wang, X. B. Zhao, *J. Power Sources* **195** (2010) 2014.

[40] Y. F. Yuan, X. H. Xia, J. B. Wu, J. L. Yang, Y. B. Chen, S. Y. Guo, *Electrochem. Comm*. **12** (2010) 890.

[41] Y. Y. Shao, J. Wang, M. Engelhard, C. M. Wang, Y. M. Lin, *J. Mater. Chem*. **20** (2010) 743.

[42] H. L. Guo, X. F. Wang, Q. Y. Qian, F. B. Wang, X. H. Xia, *ACS Nano* **3** (2009) 2653.

[43] L. Chen, Y. Tang, K. Wang, C. Liu, S. Luo, *Electrochem. Commun*. **13** (2011) 133.

[44] Y. Hu, J. Jin, P. Wu, H. Zhang, C. Cai, *Electrochim. Acta* **56** (2010) 491.

[45] Q. Cheng, J. Tang, J. Ma, H. Zhang, N. Shinya, L. –C. Qin, *Carbon* **49** (2011) 2917.

[46] Y. Jiang, Y. Lu, F. Li, T. Wu, L. Niu, W. Chen, *Electrochem. Commun*. **19** (2012) 21.

[47] G. –P. Kim, I. Nam, N. D. Kim, J. Park, S. Park, J. Yi, *Electrochem. Commun*. **22** (2012) 93.

[48] A. Kryvoruchko, L. Yurlova, B. Kornilovich, *Desalination* **144** (2002) 243.

[49] G. Duan, W. Cai, Y. Luo, F. Sun, *Adv. Funct. Mater*. **17** (2007) 644.

[50] T. Ramanathan, F. T. Fisher, R. S. Ruoff, L. C. Brinson, *Chem. Mater*. **17** (2005) 1290.

[51] Y. J. Mai, J. P. Tu, C. D. Gu, X. L. Wang, *J. Power Sources* **209** (2012) 1.

[52] S. G. Hwang, G. O. Kim, S. R. Yun, K. S. Ryu, *Electrochim. Acta* **78** (2012) 406.

[53] Y. Huang, X. Huang, J. Lian, D. Xu, L. Wang, X. Zhang, *J. Mater. Chem.* **22** (2012) 2844.

[54] J. G. Kang, Y. D. Ko, J. G. Park, D. W. Kim, *Nanoscale Res. Lett*. **3** (2008) 390.

[55] Y. Liu Y and Zhang X, *Electrochim. Acta* **54** (2009) 4180.

[56] X. Wang, C. E. Egan, M. Zhou, K. Prince, D. R. G. Mitchell and R. A. Caruso, *Chem.Comm.* **29** (2007) 3060.

[57] H. Faoucher, P. Nativo, K. Black, J. B. Claridge, M. Gass, S. Romani, A. L. Bleloch and M. Brust, *Chem.Comm*. **43** (2009) 6661.

[58] J. Cai, S. Kimura, M. Wada, S. Kuga and L. Zhang, *ChemSusChem*. **1** (2008) 149.

[59] C. Duffus, P. J. Camp and A. J. Alexander, *J. Am. Chem., Soc*. **131** (2009) 11676.

[60] H. H. Liu, X. J. Huang, B. Gu and Y. K. Choi, *J. Electroanal. Chem*. **621** (2008) 38.

[61] X. Shen, X. Chen, J. –H. Liu and X. –J. Huang, *J. Mater. Chem*. **19** (2009) 7687.

[62] K. K. R. Datta, B. Srinivasan, H. Balaram and M. Eswaramoorthy, *J. Chem. Sci*. **120** (2008) 579.

[63] J. Watanabe and M. Akashi, *J. Biomater. Sci. Polymer. Edn*. **19** (2008) 1625.

[64] W. Y. Li and L. N. Xu, *Adv. Funct. Mater*. **15** (2005) 851.

[65] N. Du, H. Zhang, B. Chen, J. B. Wu, X. Y. Ma, Z. H. Liu, Y. Q. Zhang, D. Yang, Z. H. Huang and J. P. Tu, *Adv. Mater*. **19** (2007) 4505.

[66] Y. G. Li, B. Tan and Y. Y. Wu, *Nano Lett*. **8** (2008) 265.

[67] H. J. Lui, S. H. Bo, W. J. Cui, F. Li, C. X. Wang and Y. Y. Xia, *Electrochim. Acta* **53** (2008) 6497.

[68] X. W. Lou, D. Deng, J. Y. Lee, J. Feng and L. A. Archer, *Adv. Mater*. **20** (2008) 258.

[69] J. S. Chen, T. Zhu, Q. H. Hu, J. Gao, F. Su, S. Z. Qiao and X. W. Lou, *ACS Appl. Mater. Interfaces* **2** (2010) 3628.

[70] H. Zhang, J. B. Wu, C. X. Zhai, X. Y. Ma, N. Du, J. P. Tu and D. R. Yang, *Nanotechnology* **19** (2008) 035711.

[71] D. S. Su and R. Schlogl, *ChemSusChem*. **3** (2010) 136.

[72] L. J. Zhi, Y. S. Hu, B. El Hamaoui, X. Wang, I. Lieberwirth, U. Kolb, J. Maier and K. Mullen, *Adv. Mater*. **20** (2008) 1727.

[73] J. Tang, J. L. Zhuang, L. Zhang, W. H. Wang and Z. W. Tian, *Electrochim. Acta* **53** (2008) 5628.

[74] X. H. Xia, J. P. Tu, J. Y. Xiang, X. H. Huang, X. L. Wang and X. B. Zhao, *J. Power Sources* **195** (2010) 2014.

[75] I. F. Nata, S. S. –S. Wang, T. –M. Wu and C. –K, Lee, *Soft Matter* **8** (2012) 3522.

[76] L. Kong, X. Lu, X. Bian, W. Zhang, C. Wang, W, Wang, X. Guo and Y. Yang, *ACS Appl. Mater. Interfaces* **3** (2011) 35.

[77] R. Yang, Z. Wang, J. Liu, L. Chen, *Electrochem. Solid-State Lett*. **7** (2004) A496

[78] B. Varghese, M. V. Reddy, Z. Yanwu, C. S. Lit, T. C. Hoong, G. V. S. Rao, B. V. R. Chowdari, A. T. S. Wee, C. T. Lim, C. H. Sow, *Chem. Mater*. **20** (2008) 3360.

[79] X. H. Huang, J. P. Tu, X. H. Xia, X. L. Wang, J. Y. Xing, L. Zhang, Y. Zhou, *J. Power Sources* **188** (2009) 588.

[80] B. Wang, J. L. Cheng, Y. P. Wu, D. Wang, D. N. He, *Electrochem. Comm*. **23** (2012) 5.

[81] C. Z. Wu, P. Yin, X. Zhu, C. Z. OuYang, Y. Zie, *J. Phys. Chem*. B **110** (2006) 17806.

[82] J. Z. Zhao, Z. L. Tao, J. Liang, *J. Chen, Cryst. Growth Des*. **8** (2008) 2799.

[83] X. H. Huang, J. P. Tu, C. Q. Zhang, J. Y. Xiang, *Electrochem. Comm*. **9** (2007) 1180.

[84] N. Jayaprakash, W. D. Jones, S. S. Moganty, L. A. Archer, *J, Power Sources* **15** (2012) 53.

[85] J. Shao, J. Zhang, J. Jiang, G. Zhou, M. Qu, *Electrochim. Acta* **15** (2011) 7005.

[86] H. Kim, D. -H. Seo, S. -W. Kim, J. Kim, K. Kang, *Carbon* **49** (2011) 326.

[87] M. Gao, X. Chen, H. Pan, L. Xiang, F. Wu, Y. Liu, *Electrochim. Acta* **55** (2010) 9067.

[88] I. Lahiri, S. -M. Oh, J. Y. Hwang, C. Kang, M. Choi, H. Jeon, R. Banerjee, Y. -K.Sun, W. Choi, *J. Mater. Chem.* **21** (2011) 13621.

[89] I. Paseka, *Electrochim. Acta*, **47** (2001) 921.

[90] M. Saitou, S. Oshiro, Y. Sagawa, *J. Appl. Phys*. **104** (2008) 093518.

[91] S. A. Davis, M. Breulmann, K. H. Rhodes, B. Zhang, S Mann, *Chem. Mater*. **13** (2001) 3218.

[92] S. Shinkai, K. J. C. van Brommel, A. Friggeri, *Angew. Chem., Int. Ed*. **42** (2003) 980.

[93] E. Dujardin, S. J. Mann, *Mater. Chem*. **13** (2003) 696.

[94] S. Polarz, B. Smarsly, L. Bronstein, M. Antonietti, *Angew. Chem. Int. Ed*. **40** (2001) 4417.

[95] Y. Huang, X. Huang, J. Lian, D. Xu, L. Wang, X. Zhang, *J. Mater. Chem*. **22** (2012) 2884.

[96] S. Arai, T. Saito, M. Endo, *J. Electrochem. Soc*. **154** (2007) D530.

[97] L. Tao, J. Zai, K. Wang, Y. Wan, H. Zhang, C. Yu, Y. Xiao, W. Qian, *RSC Advances* **2** (2012) 3410.

[98] X. Jia, Z. Chen, A. Suwarnasarn, L. Rice, X. Wang, H. Sohn, Q. Zhang, B. M. Wu, F. wei, Y. Lu, *Energy Environ. Sci.*, **5** (2012) 6845.

국 문 초 록

전기자동차와 휴대용 전자기기의 대중화 현상은 높은 에너지 밀도와 안정성을 지닌 리튬이온전지, 슈퍼캐패시터, 연료전지와 같은 에너지 저장 및 변환 장치의 개발을 가속화시키고 있다. 에너지시스템을 구성하고 있는 전극물질은 구조나 조성에 따라 성능이 크게 좌우되기 때문에 전극물질을 합성하기 위한 연구가 활발히 진행되고 있다. 높은 성능과 청정에너지원의 요구를 충족시키기 위하여 나노구조체를 갖는 전극물질에 대한 지난 수년간 많이 연구되었다. 특히, 최근 유·무기 복합 전극물질이 전세계적으로 주목받음에 따라 이러한 물질을 합성할 수 있는 공정개발 및 응용은 공학적인 관점에서 매우 중요한 연구분야가 되었다. 지금까지 나노구조체의 유·무기 복합 전극물질을 합성하는 많은 방법들이 연구되었으나, 상당수의 방법들은 많은 시간과 복잡한 공정을 필요로 하기 때문에 효율적인 전극물질 제조 공정의 연구와 개발이 요구된다.

이 학위논문에서는 리튬이온전지의 전극물질로 사용하기 위하여 고분자 매개체를 이용한 나노구조체 유·무기 복합물질 제조법을 제안하였다. 제조법에서 폴리에틸렌이민은 안정제, 템플레이트 및 금속 전구체를 흡착을 위한 활성점으로 사용되었으며, 아가로즈 젤은 이방성 결정구조

형성을 위한 매개체 및 탄소원으로 이용되었다. 이와 관련된 세부 결과에 대한 요악은 아래와 같다.

첫 번째, 폴리에틸렌이민을 매개로한 전기화학증착법을 이용하여 그래핀/Co_3O_4와 그래핀/NiO 필름을 합성하였다. 그래핀 옥사이드에 흡착된 폴리에틸렌이민은 양전하를 띄는 금속전구체를 잡을 수 있기 때문에 그래핀옥사이드와 금속전구체간의 복합체를 형성에 아주 중요한 역할을 수행한다. 복합체 형성을 위하여 그래핀 옥사이드를 금속전구체가 들어있는 수용액 상에 넣고 교반을 한다. 이 후, 교반된 수용액을 이용하여 전기화학증착법을 실시하였다. 제조된 물질에서 그래핀은 금속산화물 사이에 매우 고르게 분포되어 있었으며, 리튬이온전지의 음극물질로써 향상된 성능을 보여주었다.

두 번째, 높은 가역용량과 향상된 사이클 안정성을 얻기 위해 아가로스 겔을 유기주형으로 사용하여 전기화학 증착법을 통해 탄소질의 매트릭스에 박힌 형태로 존재하는 Co_3O_4와 NiO 복합체를 합성하였다. 사용된 아가로스 겔은 열처리를 통해 탄소물질로의 변환이 가능하며, 단일결정 성장에 중요한 역할을 수행한다. 합성된 물질은 분석을 통하여 연결된 기공구조를 형성하는 것이 관찰되었으며, 이방성 결정면 (111)을 나타내는 것을 확인하였다. 전기화학적 실험을 통하여 구조적인 특징의 우수성과 향상된 전기화학적 성질을 입증하였다.

주요어: 폴리에틸렌이민, 아가로즈, 코발트옥사이드, 니켈옥사이드, 나노구조체 전극, 리튬이온전지

학 번: 2011-30797

List of publications

International Publications

International Academic Published Papers (First Author)

1. M. Lee*, **G. –P. Kim***, H. D. Song, S. Park, and J. Yi, “One-step preparation of nitrogen-doped dual-porous carbon derived from used-cigarette filter for supercapacitor electrode”, Nanotechnology, Accepted. (*co-first author)
2. **G. –P. Kim**, I. Nam, S. Park, J. Park, and J. Yi, “Preparation via an electrochemical method of graphene films coated on both sides with NiO nanoparticles for use as high-performance lithium ion anodes”, Nanotechnology, 24(47), 475402 (2013).
3. **G. –P. Kim**, S. Park, I. Nam, J. Park, and J. Yi, “Synthesis of porous NiO materials with preferentially oriented crystalline structures with enhanced stability as lithium ion battery anodes”, Journal of Power Sources, 237(1), 172-177 (2013).
4. **G. –P. Kim***, S. Park*, I. Nam, J. Park, and J. Yi, “Preferential growth of Co_3O_4 anode material with improved cyclic stability for lithium-ion batteries” Journal of Materials Chemistry A, 1(12), 3872-3876 (2013). (*co-first author)
5. J. Park*, **G. –P. Kim***, I. Nam, S. Park, and J. Yi, “One-pot synthesis of silicon nanoparticles trapped in ordered mesoporous carbon for use as an anode material in lithium-ion batteries”, Nanotechnology, 24(2), 023602 (2013). (*co-first author)
6. **G. –P. Kim**, I. Nam, N. D. Kim, J. Park, S. Park, and J. Yi, “A synthesis of graphene/Co_3O_4 thin films for lithium ion battery anodes by coelectrodeposition”, Electrochemistry Communications, 22, 93-96 (2012).

International Academic Published Papers (Co-author)

1. S. Bae, H. D. Song, I. Nam, **G. –P. Kim**, J. M. Lee, and J. Yi, "Quantitative Performance Analysis of Graphite-LiFePO4 Battery Working at Low Temperature", Chemical Engineering Science, In Revision.
2. I. Nam, **G. –P. Kim**, S. Park, J. W. Han, and J. Yi, "All-solid-state, origami-type foldable supercapacitor chips with integrated series circuit analogues", Energy & Environmental Science, 7, 1095-1102 (2014).
3. Y. J. Lee, **G. –P. Kim**, Y. Bang, J. Yi, J. G. Seo, and I. K. Song, "Activated carbon aerogel containing graphene as electrode material for supercapacitor", Materials Research Bulletin, 50, 240-245 (2014).
4. I. Nam*, N. D. Kim*, **G. –P. Kim**, J. Park, and J. Yi, "One step preparation of Mn_3O_4 / graphene composites for use as an anode in Li ion batteries", Journal of Power Sources, 244, 56-62 (2013). (*co-first author)
5. S. Park, I. Nam, **G. –P. Kim**, J. W. Han, and J. Yi, "A Hybrid MnO_2 Film with Agarose Gel for Enhancing the Structural Integrity of Thin Film Supercapacitor Electrodes", ACS Applied Materials & Interfaces, 5(20), 9908-9912 (2013).
6. J. Park, W. G. Moon, **G. –P. Kim**, I. Nam, S. Park, Y. Kim, and J. Yi, "Three-Dimensional aligned mesoporous carbon nanotubes filled with Co_3O_4 nanoparticles for Li-ion battery anode applications", Electrochimica Acta, 105, 110-114 (2013).
7. J. Park, **G. –P. Kim**, H. N. Umh, I. Nam, S. Park, Y. Kim, J. Yi, "Co_3O_4 nanoparticles embedded in ordered mesoporous carbon with enhanced performance as an anode material for Li-ion batteries", Journal of Nanoparticle Research, 15(9), 1943 (2013).
8. Y. J. Lee, H. W. Park, **G. –P. Kim**, J. Yi, and I. K. Song, "Supercapacitive electrochemical performance of graphene-containing carbon aerogel prepared using polyethyleneimine-modified graphene oxide", Current Applied Physics, 13(5), 945-949 (2013).
9. I. Nam, S. Park, **G. –P. Kim**, J. Park, and J. Yi, "Transparent and ultra-bendable all-solid-state supercapacitors without percolation problems", Chemical Science, 4(4), 1663-1667 (2013).

10. S. Park*, I. Nam*, **G. –P. Kim**, J. Park, N. D. Kim, Y. Kim, and J. Yi, “A brain-coral-inspired metal-carbon hybrid synthesized using agarose gel for ultra-fast charge and discharge supercapacitor electrodes”, Chemical Communications, 49(15), 1554-1556 (2013). (*co-first author)
11. I. Nam, **G. –P. Kim**, S. Park, J. Park, N. D. Kim, and J. Yi, “Fabrication and design equation of film-type large-scale interdigitated supercapacitor chips”, Nanoscale, 4(23), 7350-7353 (2012).
12. N. D. Kim, S. J. Kim, **G. –P. Kim**, I. Nam, H. J. Yun, P. Kim, and J. Yi, “NH_3-activated polyaniline for use as a high performance electrode material in supercapacitors”, Electrochimica Acta, 78, 340-346 (2012).
13. I. Nam, N. D. Kim, **G. –P. Kim**, J. Park, and J. Yi, “Amorphous Mn Oxide-Ordered Mesoporous Carbon Hybrids as a High Performance Electrode Material for Supercapacitors”, Journal of Nanoscience and Nanotechnology, 12(7), 5704-5708 (2012).
14. S. –M. Jeong, M. K. Kim, **G. –P, Kim**, T. Y. Kim, and S. –H. Baeck, “Preparation of Pt-Au/carbon catalysts by a reduction method and their electrocatalytic activities for oxygen reduction reactions”, Chemical Engineering Journal 198, 435 (2012).
15. K. –H. Kim, K. S. Kim, **G. –P. Kim**, and S. –H. Baeck, “Electrodeposition of mesoporous ruthenium oxide using an aqueous mixture of CTAB and SDS as a templating agent”, Current Applied Physics, 12, 36 (2012).
16. K. –H. Kim, **G. –P. Kim**, I. K. Song, K. –H. Yang, B. C. Lee, and S. –H. Baeck, “Investigation of electrochemical properties of RuO2 thin films modified by e-beam irradiation” Thin Solid Films, 519, 3086 (2011)

International Academic Papers in Preparation

1. **G. –P. Kim**, S. Bae, H. D. Song, M. Lee, and J. Yi, “Decoration of Bio-Inspired Nanospheres with Pt Nanoparticles via Polymer-Assisted Strategy for Enhanced Electrocatalytic Activity”, in preparation (2014).

2. **G. –P. Kim**, Y. J. Lee, S. Bae, I. K. Song, and J. Yi, “Synthesis of chemically modified carbon support for platinum electrocatalysts”, in preparation (2014).
3. W. G. Moon*, **G. –P. Kim***, M. Lee, H. D. Song, and J. Yi “Quasi-solid-state agarose gel electrolyte for flexible supercapacitor” in preparation (2014). (*co-first author)

International Conferences (First author)

1. **G. –P. Kim**, S. Bae, W. G. Moon, J. Park, I. Nam, S. Park, and J. Yi, “Synthesis of chemically modified carbon support for platinum electrocatalysts”, The 14th Japan-Korea Symposium on Catalysis, WINC Aichi, Nagoya, Japan, July 1-3 (2013)
2. **G. –P. Kim**, S. Park, I. Nam, J. Park, N. Kim, H. Song, and J. Yi, “Facile synthesis of Co_3O_4 nanoflakes embedded in 3D porous carbon matrix for lithium ion battery anodes by electrodeposition”, 244th American Chemical Society National Meeting & Exposition, Philadelphia, Pennsylvania, USA, August 19-23 (2012).

International Conferences (Co-author)

1. S. Park, I. Nam, **G. –P. Kim**, M. Lee, W. G. Moon, S. Bae, and J. Yi, “Robust hybrid film containing pseudocapacitive MnO_2 for large areal capacitance”, 247th American Chemical Society National Meeting & Exposition, Dallas, Texas, USA, Mar. 16-20 (2014)
2. I. Nam, S. Park, **G. –P. Kim**, H. D. Song, W. G. Moon, S. Bae, and J. Yi, “Fabrication of Transparent and Flexible Supercapacitor”, 2013 MRS Fall Meeting Program & Exhibit, Boston, Massachusetts, USA, Dec. 1-6 (2013)
3. I. Nam, S. Park, **G. –P. Kim**, J. Park, N. D. Kim, I. K. Song, and J. Yi, “Design and preparation of innovative supercapacitors for energy storage systems”, 245th ACS National Meeting & Exposition, New Orleans, Louisiana, USA, April 7-11 (2013)
4. I. Nam, N. D. Kim, J. Park, **G. –P. Kim**, S. Park, and J. Yi, “Environmentally Benign Synthesis of a Mn_3O_4/Graphene Hybrid Material for Use as an Anode in Li

Ion Batteries", 16th International Meeting on Lithium Batteries, ICC Jeju, Korea, June 17-22 (2012)

5. I. Nam, N. D. Kim, **G. –P. Kim**, J. Park and J. Yi, "Use of ordered mesoporous carbons with MnO2 for supercapacitor", NANO KOREA 2011, KINTEX, Korea, August 24-26 (2011)

Domestic Conferences

1. 이민재, **김길표**, 송현돈, 박수민, 문원균, 이종협, "사용된 담배필터를 재활용한 기공성 탄소제조 및 수퍼커패시터 성능평가", 2014년 한국청정기술학회 춘계 학술발표회, 여수경도리조트, 3. 27-28 (2014)
2. 배성준, 송현돈, 남인호, **김길표**, 이종민, 이종협, "수치해석을 통한 리튬이온 전지 활물질 특성 평가", 2014년 한국청정기술학회 춘계 학술발표회, 여수경도리조트, 3. 27-28 (2014)
3. 남인호, **김길표**, 박수민, 한정우, 이종협, "패턴화를 통한 고전압 수퍼커패시터 시스템", 2014년 한국청정기술학회 춘계 학술발표회, 여수경도리조트, 3. 27-28 (2014)
4. 남인호, **김길표**, 박수민, 송현돈, 이민재, 문원균, 배성준, 이종협, "대면적의 패턴화된 망간 산화물 수퍼커패시터 개발 및 성능 평가", 한국전기화학회 2013년 추계 총회 및 학술발표회, 대전컨벤션센터, 11. 7-9 (2013)
5. 박수민, 남인호, **김길표**, 문원균, 배성준, 이민재, 송현돈, 이종협, "박막전지의 구조적 안정성을 높이기 위한 유기겔-금속산화물 복합체 합성", 한국전기화학회 2013년 추계 총회 및 학술발표회, 대전컨벤션센터, 11. 7-9 (2013)
6. **김길표**, 박수민, 남인호, 송현돈, 이민재, 배성준, 문원균, 이종협, "전기화학 증착법을 이용한 이방성 결정구조를 지닌 연결된 기공구조의 NiO 합성 및 리튬이온 배터리 음극 활용", 한국전기화학회 2013년 추계 총회 및 학술발표회, 대전컨벤션센터, 11. 7-9 (2014)
7. 문원균, 박준수, **김길표**, 남인호, 박수민, 이종협, "삼차원으로 정렬된 탄소 나노튜브/산화코발트 합성 및 리튬이온전지 음극물질로의 응용", 한국

화학공학회 2013년도 가을 총회 및 학술대회, 대구 EXCO, 10. 23-25 (2013)

8. 이윤재, 송인규, 이중원, **김길표**, 이종협, 윤중락, “카본 에어로겔-그래핀 화합물의 합성 및 슈퍼커패시터 전극으로 응용에서 PEI(polyethyleneimine) 처리된 산화 그래핀의 양이 전기화학적 물성에 미치는 영향”, 한국화학공학회 2013년도 가을 총회 및 학술대회, 대구 EXCO, 10. 23-25 (2013)
9. 남인호, 박수민, **김길표**, 문원균, 배성준, 송현돈, 이종협, “아가로스 겔을 이용한 삼차원 금속/탄소 복합체 제조 및 고출력 슈퍼커패시터로의 응용”, 2013년 한국청정기술학회 추계 학술발표회, 제주 한화리조트, 9. 25-27 (2013)
10. 이윤재, 홍웅기, **김길표**, 윤중락, 이종협, 송인규, “PEI(polyethyleneimine)로 처리된 산화 그래핀을 이용한 카본 에어로젤-그래핀 화합물의 합성 및 슈퍼커패시터 전극 물질으로써의 응용”, 한국화학공학회 2013년 봄 총회 및 학술대회, 광주 김대중컨벤션센터, 4. 24-26 (2013)
11. 박수민, 남인호, **김길표**, 박준수, 배성준, 이종협, “고출력 슈퍼커패시터 전극을 위한 삼차원 구조의 금속/탄소 복합체 제조”, 한국전기화학회 2013년도 춘계총회 및 학술발표회, 창원컨벤션센터, 4. 11-13 (2013)
12. 남인호, **김길표**, 박수민, 박준수, 문원균, 이종협, “망간 산화물과 그래핀 복합체를 이용한 리튬 이온 전지의 음극 재료 개발”, 한국전기화학회 2013년도 춘계총회 및 학술발표회, 창원컨벤션센터, 4. 11-13 (2013)
13. **김길표**, 박수민, 남인호, 박준수, 송현돈, 이종협, “Agarose Gel-Mediated Electrodeposition: Preferential Growth of Co_3O_4 anode material for Lithium-Ion Batteries”, 한국전기화학회 2013년도 춘계총회 및 학술발표회, 창원컨벤션센터, 4. 11-13 (2013)
14. **김길표**, 박수민, 남인호, 박준수, 이종협, “아가로스 겔 주형을 이용한 연결된 기공구조를 갖는 니켈옥사이드 합성 및 리튬 이차전지 음극 활물질 응용”, 2013년 한국청정기술학회 춘계 학술발표회, 여수 경도리조트, 3. 28-29 (2013)
15. 박수민, **김길표**, 남인호, 박준수, 배성준, 문원균, 이종협, “금속 산화물/유기겔 하이브리드 전극 제조와 박막형 슈퍼커패시터에의 응용”, 2013년 한국청정기술학회 춘계 학술발표회, 여수 경도리조트, 3. 28-29 (2013)

16. 남인호, 김남동, **김길표**, 박준수, 박수민, 이종협, “고효율 커패시터를 위한 비정질 산화망간과 중형기공성탄소 복합체 제조”, 춘계 한국청정기술학회, 연세대학교, 5.25 (2012)
17. 김남동, 김소정, 박준수, **김길표**, 남인호, 박수민, 김필, 이종협, “슈퍼캐패시터의 전기화학적 성능 증가를 위한 질소도핑방법의 개발”, 한국화학공학회 봄 총회 및 학술대회, 제주국제컨벤션센터, 4.25-27 (2012)
18. 박준수, **김길표**, 김남동, 남인호, 박수민, 이종협, “실리콘 나노입자가 담지된 중형기공성 탄소체의 합성: 리튬 이차전지 음극 활물질 응용”, 한국화학공학회 봄 총회 및 학술대회, 제주국제컨벤션센터, 4.25-27 (2012)
19. 남인호, 김남동, 박준수, **김길표**, 박수민, 이종협, “비결정성 망간 산화물과 중형 기공성 탄소의 복합체 제조 및 수퍼커패시터 전극 활용”, 한국전기화학회 춘계총회 및 학술발표회, 광주광역시 김대중컨벤션센터, 4.12-14 (2012)
20. **김길표**, 김남동, 박준수, 남인호, 박수민, 이종협, “리튬 이차전지 음극 활물질 응용을 위한 그래핀/코발트 옥사이드 물질의 제조와 분석”, 한국전기화학회 춘계총회 및 학술발표회, 광주광역시 김대중컨벤션센터, 4.12-14 (2012)
21. 박준수, 엄하늬, **김길표**, 김남동, 남인호, 박수민, 김영훈, 이종협, “리튬 이차전지용 Co_3O_4/중형기공성 탄소 복합체의 전기화학적 특성”, 한국전기화학회 춘계총회 및 학술발표회, 광주광역시 김대중컨벤션센터, 4.12-14 (2012)
22. 남인호, 김남동, 박준수, **김길표**, 이종협, “비결정성 망간 옥사이드-중형기공성 탄소 하이브리드 제조 및 전기화학 커패시터로의 활용”, 추계 한국화학공학회, 송도컨벤시아, 10. 26-28 (2011)
23. 김남동, 윤형진, 남인호, 박준수, **김길표**, 이종협, “비정질 결정 구조를 가지는 망간 산화물의 산화수 조절을 위한 방법”, 추계 한국화학공학회, 송도컨벤시아, 10. 26-28 (2011)
24. 김남동, 윤형진, 남인호, 박준수, **김길표**, 이종협, “전기화학 커패시터의 전극 물질 활용을 위한 비정질 망간 산화물의 제조”, 추계 한국에너지공학회, 서울대학교 교수회관, 10. 20-21 (2011)

25. 남인호, 김남동, 박준수, **김길표**, 이종협, “수퍼커패시터 전극 활용을 위한 중형기공성 탄소와 비정질 망간산화물의 복합체 제조”, 추계 한국에너지공학회, 서울대학교 교수회관, 10. 20-21 (2011)
26. **김길표**, 김남동, 박준수, 남인호, 이종협, “3차원 대형기공 구조를 갖는 니켈코발타이트 음극 물질 합성”, 춘계화학공학회, 창원컨벤션센터, 4. 27-29 (2011)